3 Physics and Technology of Fusion

Work in fusion plasma physics and technology includes 20 tasks. The tasks are grouped under the six following sub-headings corresponding to the EFDA Task Forces and Topical Groups:

- Integrated tokamak modelling
  - Support of the workflow orchestration system for fusion modelling
  - Tokamak modelling
  - Nonlinear dynamics of fast ion driven plasma modes near instability threshold – theoretical basis for integrated tokamak modeling
  - Stochastic processes and stochastic representations for the kinetic equations of a gas of charged particles

- Plasma-wall interaction
  - Portable LIBS device for calibrated measurements of material deposition and composition of the walls on plasma source
  - Study of laser based diagnostic methods, photonic cleaning and spectroscopy (including LIBS) in perspective of next-step fusion devices (including ITER)
  - Spectroscopic and ion diagnostics for laser-induced removal of fuel and co-deposits from PFCs in tokamaks
    Including:
    - Removal of the deposited materials by laser ablation techniques. Investigation of carbon layers with varying concentrations of Al (Be analogue), W and W-Be
    - Investigation of film break-up processes during laser cleaning. Monitoring of the composition of gases and particles released from the target
    - Irradiation of TEXTOR and AUG samples containing material mix of carbon and tungsten by the Nd:YAG pulsed repetitive laser. Use of optical spectroscopy together with ion diagnostics to characterize chemical composition of samples
    - Photonic cleaning methods
    - Conversion of deposits to dust
  - Studies of material erosion and re-deposition on plasma facing components from the present day machines. Characterization of exposed PFCs with various microscopic and analytical techniques (TEXTOR and AUG)
    Including:
    - Dust generation in present devices
    - Characterisation of outer and inner divertor erosion as well as the migration of impurities from main chamber to divertor and inside the divertor
    - PWI in a full-W device

- Development of material science and advanced materials for DEMO
  - Ab-initio study of defects configurations and their interactions in W-Ta and W-V model alloys
  - W/steel joints fabrication route based on pulse plasma sintering (PPS) method and explosive bonding
  - Hydrostatic Extrusion (HE) processing of ODS ferritic steel: microstructure characterisation, mechanical properties and thermal stability
  - Application of Mössbauer spectroscopy to Fe alloys characterization
  - Mathematical modelling of thermal-hydraulic problems related to the HTS

- Fusion plasma diagnostics
    - Activation technique in a cross-check experiment for high resolution neutron spectrometry
    - Diamond and track detectors to detect escaping fast alpha particles
    - Cherenkov detectors for fast electron measurements: new diagnostics for Tore-Supra
    - High-temperature Hall sensor for future applications in measurements of magnetic field in fusion reactors
    - Localized plasma polarimetry based on the phenomenon of normal modes conversion
    - Development of gas detectors for 2.5 and 14 MeV neutron measurements utilizing activation method and for soft X-ray detection
- Inertial fusion energy “keep-in-touch” activity
    - Analysis of emerging options of IFE on the basis of results of experiments and numerical modelling

3.1 Integrated Tokamak Modelling

Support of the workflow orchestration system for fusion modelling

Corresponding author **Marcin Płóciennik**
marcinp@man.poznan.pl

The main goal of this activity was the support of the workflow orchestration system (based on Kepler) for fusion modelling. This was realised under the ITM-TF activities.
As part of the implementing tools to do comprehensive simulations, the ITM-TF identified the need for workflow orchestration tools and for mechanisms to transfer data between the modules that is independent of the computer language in which the modules are written, and that is capable of transferring data between modules running on the same node, on the same cluster, and on widely separate compute resources including HPC and GRID resources. The selected scientific workflow orchestration system Kepler is designed to help scientists, analysts, and computer programmers create, execute, and share models and analyses across a broad range of scientific and engineering disciplines. The Kepler software helps users share and reuse data, workflows, and components developed by the scientific community to address common needs.

The activity of the support of the workflow orchestration system activity in 2010 included the following tasks:

- Provision of the tutorials of the usage of the workflow orchestration system and tools, usage of the HPC and Grid resources
- Support of workflow scenarios
- Support of the services for the Grid/HPC access
- Support of the inclusion of template Grid/HPC workflows into ITM workflows

Provision of the tutorial of the usage of the workflow orchestration system and tools, usage of the HPC and Grid resources.

Kepler hands-on tutorial was conducted by Marcin Płóciennik and Michał Owsiak during ITM General meeting 13-17.09.2010 in order to provide ITM members with knowledge related to Kepler itself as well as workflow concepts and their basic usage. The more advanced part concerned the ITM specific workflows and the Grid and HPC access.

There were 3 separate parts of the tutorial, each taking 4 hours:

- Part1: Introduction to Kepler - basic knowledge about Kepler, building basic workflows, debugging
- Part2: ITM Workflows in Kepler - building the example ITM Workflows
- Part3: GRID and HPC Access through Kepler

All materials and exercises are available on-line: http://serpens.psnc.pl/itm

They can be used in order to access GRID/HPC resources. Template workflows are designed in such a way that minimal interference from a user is required. Template workflows are based on the concept of so called composite actors.

Tokamak modelling

Corresponding author **Roman Stankiewicz**
roman.stankiewicz@ifpilm.pl

The effort to develop modular system of codes, modeling various physical processes, has been undertaken in TF-ITM project. The modules should be implemented in the frame of data processing system KEPLER. The participation in TF-ITM Project 3 in developing ETS (European Transport Solver) is presented in this report. The ETS was tested for cases of transport barrier and stiff problem. For some transport model the diffusion coefficient depends nonlinearly on gradient of the solution. In this case the numerical instabilities can appear for the acceptable small time step. The several methods of the suppression of the numerical instability was considered. The work in this field will be continued next year.

The ITS (Impurities Transport Solver) was tested by comparing the results of the codes ETS/ITS with the results of the codes Jetto/Sanco. The Amns data obtained from ADAS has been included into ITS. The Kepler actor was generated for ITS and included into general Kepler workflow.

Test of ETS for case of transport barrier.
The testing of barrier dynamics was performed for single diffusion equation in cylindrical geometry for two models of diffusion. In the first model the diffusion coefficient is discontinuous with discontinuity position defined by critical value of e-folding length

$$D_i = D_1 \quad \text{for} \quad -\frac{n_i}{(\partial n_i / \partial \rho)} > L_{cr}$$

and $D_i = D_2 << D_1$ for $-\frac{n_i}{(\partial n_i / \partial \rho)} < L_{cr}$

In the second model the diffusion is defined by function $D=D_0 + D_1/(1+(|n'|/n'_{cr})^n)$. The dynamics was considered for two scenario:

- the source term increased in time
- constant source and initial distribution function *n* equals zero.

The numerical results are compare with the analytical ones obtained by manufactured solution method. The obtained results using solver 3 and solver 7 from ETS reproduced the position of the barrier with significant error The decreasing of mesh size and time step only partly reduced the error.

Stiff transport problem
For the stiff transport model the several method of suppression of numerical instability was consider. In the first method the extra diffusion term is introduced and compensated by source term defined by the solution from previous time step.

$$\frac{\partial \rho n}{\partial t} - \frac{1}{\rho}\frac{\partial}{\partial \rho}\left(\rho(D_1 + D_{ad})\frac{\partial n}{\partial \rho}\right) = S - \frac{1}{\rho}\frac{\partial}{\partial \rho}\left(\rho D_{ad}\frac{\partial n_{old}}{\partial \rho}\right)$$

In the second method the compensation is done by extra convection term.

$$\frac{\partial \rho n}{\partial t} - \frac{1}{\rho}\frac{\partial}{\partial \rho}\left(\rho(D_1 + D_{ad})\frac{\partial n}{\partial \rho} - Vn\right) = S \qquad V = D_{ad}\frac{\partial n_{old}/\partial \rho}{n_{old}}$$

$$D = 0.1 + (|n'| - n'_{cr})^{0.5} H(|n'| - n'_{cr})$$

The smoothing procedure can be used to check if the numerical instability is suppressed.

The results for the first method are presented below. The solution and space derivative of the solution for initial distribution equals zero and for time equal 1 s. It follows from the results that for presented case the time step can be increased by two order with preserving the accuracy.

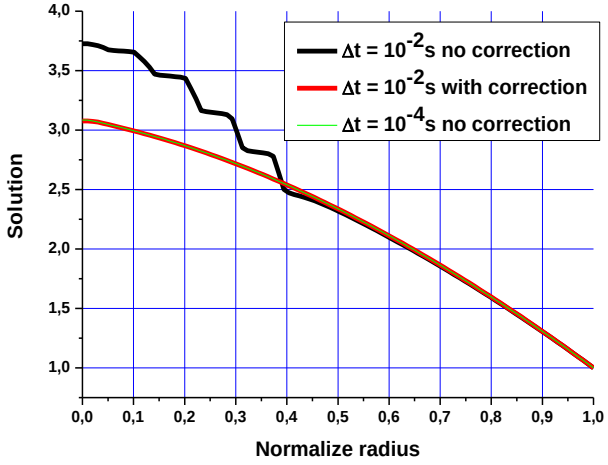

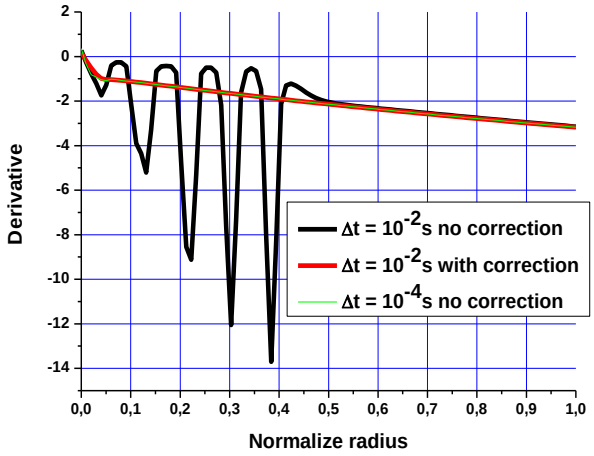

The work will be continued in order to have the procedure able to adjuste automatically the time step and the value of extra diffusion .

Impurity transport solver

ITS solves the 1.5D transport equations for the density of each ionization state for each impurity. Different ionization states are coupled by the ionization and recombination processes. The time step is divided into two subintervals. In the first half step the equation are solved starting from the lowest ionization stage to the highest ionization stage. In the second half step, the 1D equation are solved starting form the highest ionization stage to the lowest one. In the solution of each ionisation stage the new value of impurity density calculated in previous ionization stage is used.

ITS was tested by comparing the results of the codes ETS/ITS with the results of the codes Jetto/Sanco. The Amns data obtained from ADAS has been included into ITS. The Kepler actor was generated for ITS and included into general Kepler workflow.

Nonlinear dynamics of fast ion driven plasma modes near instability hreshold – theoretical basis for integrated tokamak modelling

Corresponding author **Paweł Berczyński**
Pawel.Berczynski@ps.pl

The source of the energetic particles in fusion plasmas can be nuclear reactions, e.g. in ITER energetic alpha particles will be produced in D-T nuclear reactions. In present day experiments high-energy particles arise mainly due to plasma heating using ICRH (ion-cyclotron resonance heating) and NBI (neutral beem injection) methods. The non-equilibrium distributions of the fast ions may lead to the occurrence of wave micro-instabilities, which may have direct impact on the operation scenarios and ignition conditions. The investigation of the initial phase of these instabilities is connected with the identification of the stability thresholds with respect to wave excitations by fast ions. The model describing the nonlinear evolution of a single plasma wave mode driven resonantly by fast ions just above the linear instability threshold, the Berk and Breizman (BB) model, was developed in a number of papers, and was applied to study the dynamical properties of both the Toroidal Alfven Eigenmodes (TAE) and the fishbone instability excited by energetic ions in tokamak plasmas. The model has been used to interpret real tokamak experiments.

In 2010 in the framework of the project the existing Berk-Breizman (BB) model which describes the evolution of a single coherent plasma wave was generalized for the case of two-plasma modes. Different relaxation processes described by different collision operators such as Krook, diffusion and dynamical friction (drag) collision models have been taken into account. A system of two coupled integro-differential equations for the mode amplitudes has been derived and examined numerically. Depending on the type of relaxation process different nonlinear regimes have been observed. It is found that in the case, when the dominant relaxation processes are modeled via the Krook or diffusion collision operators, the non-linear evolution of the wave amplitude may exhibit four main regimes: a steady-state, periodic amplitude modulation, chaotic and explosive regimes. This is in contrast to the case when dynamical friction is the dominant collision process, where the explosive evolution of the wave amplitude was found to be the only possible behavior, i.e. within the context of the perturbation theory the mode reaches arbitrarily large amplitude in a finite time. In addition, it is found that the finite separation in the phase velocities of the two modes weakens the interaction strength between the modes.

The presented extension of the BB model to the two mode case with different collisions models has been done as one of our attempts to develop the method suitable to describe the multi-mode case of many isolated waves. The fully multi-mode case including different collision models is a complicated task and still remains further investigations.

Stochastic processes and stochastic representations for the kinetic equations of a gas of charged particles

Corresponding author **Witold Karwowski**
witoldkarwowski@go2.pl

The study of random processes of diffusion in R^n and jumps on a fractal $\Gamma \subset R^n$ in terms of the Dirichlet forms E carried out in 2009 has been continued in 2010. We recall that the jump measure *J* of the Dirichlet form was defined as an image of a jump measure *j* of a process in a non-Archimedean metric space. It then follows that the jump intensity depends on the hierarchical structure of Γ rather then the geometric distance in R^n. For a class of fractals in R^2 we have found a condition on the measure *j* so that the Dirichlet form E is regular. The condition is given in terms of Hausdorff dimension of Γ. This was obtained in 2009 but the reasoning was applicable only to the fractals Γ such that their images under different contraction similarities did not overlap. In 1010 it has been shown that the results are valid even if the two images do overlap provided their intersection has vanishing Lebesgue measure.

The work of 2009 and 2010 are presented in the paper: W. Karwowski, K. Yasuda *Dirichlet Forms for Diffusion in* R^2 *with Jumps on Fractals: The regularity problem.* p-adic Numbers, Ultrametric Analysis and Applications **2**, (2010) 341-359.

3.2 Plasma-Wall Interaction

Portable LIBS device for calibrated measurements of material deposition and composition of the walls on plasma source

Corresponding author **Monika Kubkowska**
monika.kubkowska@ipplm.pl

Among other candidate methods, Laser Induced Breakdown Spectroscopy (LIBS) offers the possibility of non-contact real-time measurements of contents of different components in a sample under analysis. This specific feature looks to be very convenient in perspective of in-vessel tokamak monitoring of the fuel retention in plasma facing components. Moreover, flexibility of the method allows for a distant observation of the laser induced plasma and easy transmission of the signal to detectors with the use of fibers. To assess the possibilities of the method, the task was aimed on investigation calibrated samples and comparison of the results obtained by collaborating laboratories.
The investigated samples were produced by magnetron sputtering by NILPRP, Romania and contained material mix relevant to the one foreseen for components of the next step fusion devices. Glow Discharge Optical Spectrometry (GDOS) was used as a quality control technique for measurement of the coating thickness and impurities under production conditions. In particular two sets of samples have been investigated:

- Titanium substrates with 10 μm tungsten layer with 1-2 μm Molybdenum interlayer. Carbon and oxygen as surface contamination.
- Titanium with C:W layers of two fixed ratios contaminated with O on the surface.

The experiments with the use of the Mechelle5000 spectrometer equipped with iCCD camera of the laser plasma generated by 3-3.5 ns, 300 mJ pulses of Nd:YAG laser system operating on 1064 nm wavelength with repetition rate up to 10 Hz allowed for reliable qualitative analysis of all samples and for preliminary estimation of the calibration curve for carbon component in the samples of the second type.

The main part of the experiment was carried on with a beam of power density of 5 MW/cm^2. In case of the presence of carbon it was important to adjust a proper value of time delay (time between the laser pulse and start of acquisition) which had to be short enough to observe recombination of speedily propagating carbon ions. The delay at level of 100 ns was applied. To reconcile observation of carbon lines and tungsten which appears later (about 300-500 ns after laser pulse in applied experimental conditions) relatively long acquisition time has been used – 500 ns. Comparison of spectra evolution for two types of samples with 70 and 82 % of carbon are presented in fig.1.

Integration of the lines of carbon for subsequent shots, in the same irradiation and optical system collection conditions, in samples with different composition ratio of carbon allowed for the estimation of the calibration curve (line) for line intensity in dependence on carbon ratio in the range from 70 to 82 %. The curve is presented in fig. 2.

The results gathered at this stage of experiment allowed for a proper qualitative analysis of the sample and for an attempt to estimate a calibration curve for carbon in a narrow range of concentration, however, further experiments and study are needed for quantitative analysis of the samples. Nevertheless, as far as the present study was firm to assess, such an analysis is possible mainly due to a good stability of the signals attributed to different components in most of the experiments (in which variations of the line magnitudes in steady conditions were not higher than 10 % in subsequent shots).

Although in described experiments, the set-up with a plasma observation in parallel direction to the target was applied, it is more advisable to study set-up with collinear plasma observation (i.e. in direction of the laser beam). Such a set-up was successfully tested in other experiments at IPPLM and gave repetitive results, however, with a bit worse S/N ratio. The optimistic premise for such a set-up is

that in the real device diagnostics will work in high vacuum conditions in which the influence of the background is less deteriorating for the measurement signal.

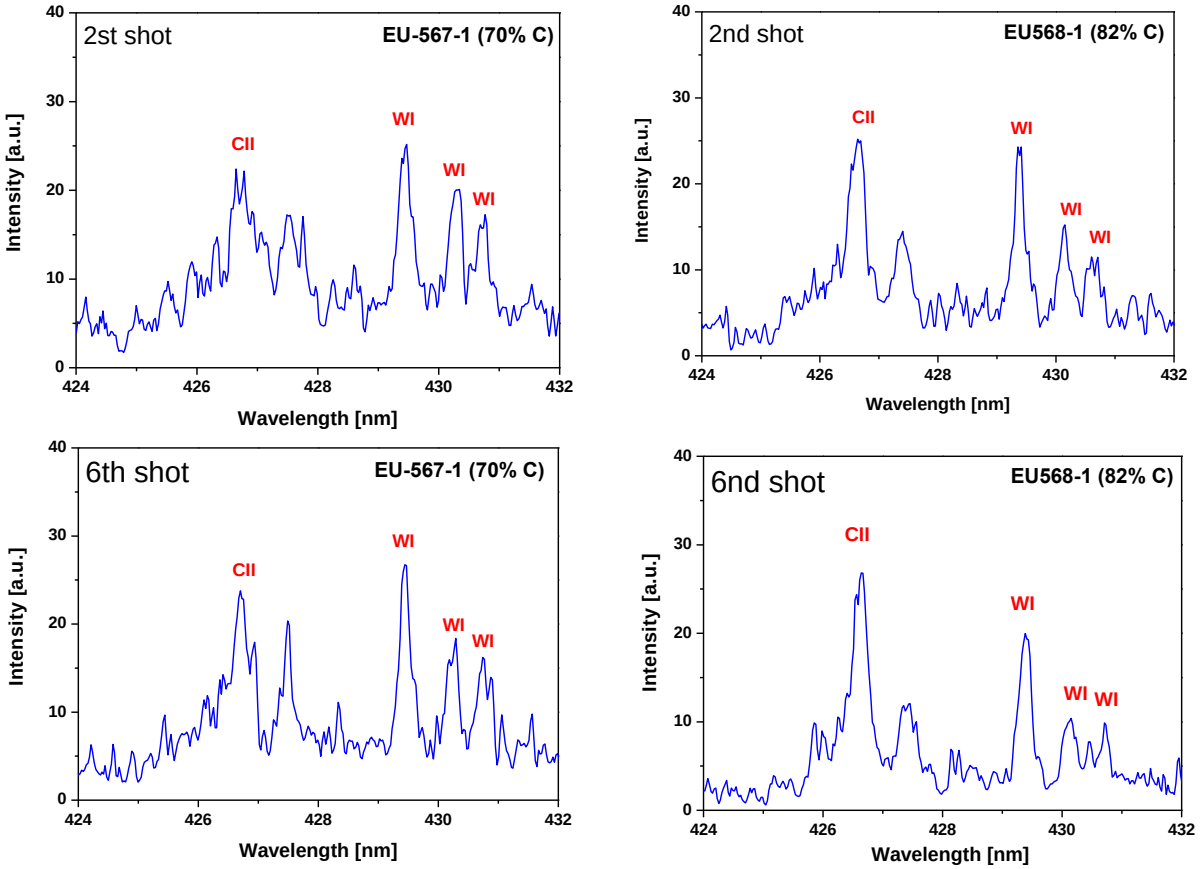

Fig.1 Comparison of spectra evolution for samples with different C concentration

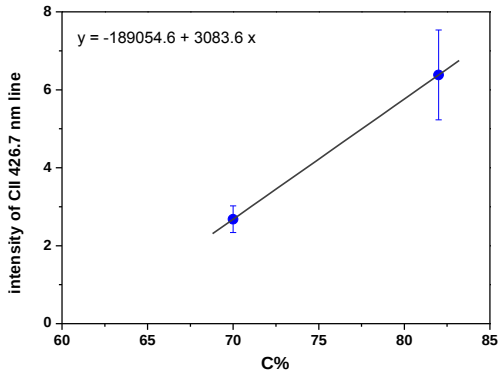

Fig. 2 Calibration curve for carbon ratio in linear dynamic range

The attempt of estimation of the calibration curve was a natural step in the project and even it was not very firm it was a big step forwards, because the features of the laser induced plasma appeared to be stable enough to give results in a reasonable range of confidence. The clearly difference between the spread of obtained intensities of Carbon line for both calibrate samples is seen. The reason could be a fact that sample contained 82 % of Carbon was prepared with larger inaccuracy. The further steps should be aimed on the broadening of the calibration range for carbon (which is accompanied with co-deposition in present device) and on estimating of such curves for hydrogen isotopes which is a goal of this task itself.

Study of laser based diagnostic methods, photonic cleaning and spectroscopy (including LIBS) in perspective of next-step fusion devices (including ITER)

Corresponding author **Monika Kubkowska**
monika.kubkowska@ipplm.pl

The project consisted of three following tasks: Divertor Erosion Monitor study, review of the spectroscopic diagnostics foreseen in ITER, and study of periodic dust mobilization from hot surfaces with the use of laser scanning method.
The system for monitoring divertor erosion is of a great importance for ITER as it gives not only information on the condition of the divertor wall which is required for its maintenance but also helps to estimate the amount of material which was removed from the wall and may influence plasma operation as well as safety issues.

The basic feature of such a system is the need of remote operation which makes laser-based and in general, optical non-contact techniques favorable. Laser beams make it possible to probe distant surfaces and moreover do not provide any interference with other systems and are immune against interference resulted from electromagnetic fields. The laser and optical market offers a variety of solutions in terms of laser sources, detectors, waveguides and other optical elements which make it possible to develop a strictly specialized system for given requirements.

Independently on advanced and flexible components laser technology offers the advantage of a few methods with countless variants to measure the quantities of interests which, in case of ITER, divertor are displacement, deformation, thickness/distance difference and vibration with time and spatial resolution dependent on the method, variant and parameters of the used equipment.

In case of the development of the diagnostic system, besides of such issues as demanded accuracy, resolution, operating speed and the range of quantities which are to be measured, the main concern is in the integration of the diagnostics with the device, which part it will constitute. In ITER it is a special issue as the characteristics of the device are rather uncommon with most of available applications. The issue is not only in the specific conditions of thermonuclear device but also in strict spatial conditions also due to presence of other diagnostic and maintenance systems which cannot be interfered by the divertor erosion monitor.

In preparation of the diagnostic system for such a device as ITER, one should also take into account that the other components, although they were designed, are not yet built and mounted which entails some unexpected modifications to the full set-up. To be up to this risk the system should offer enough flexibility to have its set-up modified without lost of performance or in other case to have enough excess in parameters which could be given up while demands are still satisfied.

The basic problem in application of any laser method for ITER is vibration which, if not being dealt with, would corrupt any results for erosion measured as a displacement of the wall surface. Without knowledge about the parameters of the vibration at this stage, we must be prepared that its amplitude will be significantly higher component in the common optical signal than the component which can be attributed to erosion. Moreover, we cannot be sure if the vibration will have a harmonic character, what frequency components it can include or what will be its boundary frequency. As the remedy for this problems only precise measurements of the vibration may be applied.

The most popular approach for the vibration measurement is application of vibration sensors which, in fact, measure the acceleration of the object they are mounted in and are called accelerometers. Many types of the miniature accelerometers which can be mounted inside mechanical components are commercially available. They offer measurements of vibration in range of single Hz to kHz and acceleration even higher than 500 g. Commercially available miniature vibration sensors have dimension not exceeding 1 cm which maybe would allow to mount such sensors on the back side of the

wall and in the head of DEM (as we cannot expect that vibration in this location is the same in terms of the amplitude and phase as the one in the wall). The sensors provide an electrical signal dependent on the magnitude of the acceleration which makes it possible to measure amplitude and phase of the vibration. Application of such sensors would not only make the evaluation of erosion rate with the use of laser techniques much easier but would also provide very useful information of the vibration of the components of the device. Such an information would be very convenient for example for evaluation of mechanical stresses and also wear of mechanical components especially in significantly more intensive exploitation than it takes place in presently operating thermonuclear devices.

Another issue is the location of the set-up elements themselves. The solution which offers the best flexibility is putting the device with collection optics under the dom and providing all necessary signals in an optical form with the use of fibers, but if the solution is not possible, the device may be also port-plugged. Regardless of the location the device should be screened against electromagnetic fields which can be obtained by application of a special box designed by an expert.

For installation of a optical diagnostic system in a tokamak, an important issue is also concerned on deterioration of the optical components due to deposition of contamination. Due to this a possible solution can be offered which relies on application of a high-powered pulsed fiber laser for cleaning of the elements. The fiber lasers offer a choice of adjustment of power density which may remove deposits from windows and mirrors without damaging the elements themselves, however its value depends on the properties of the deposits which are not known at the moment with a satisfactory accuracy. Nevertheless the optimal parameters of the laser beams can be adjusted later due to a great flexibility in control of lasing parameters in fiber system.

Fig. 1 An arm for laser scanning inspection system provided by ROMER

Industry offer in the field of laser measurements of distance includes a variety of devices which provide satisfactory parameters for DEM for ITER. Instruments of companies as Metron, LDI, Romer, Capture3D, Nvision and others offer remarkable resolution, accuracy and time resolution. The products contain not only apparatus but also software with extensive capabilities as automatic searching for areas of given properties or generating so called ‘wather maps’. A sample photo of a set-up provided by ROMER is presented in fig 1. Disadvantage of application of such a device is its adaptation for DEM needs as commonly they are used on stages with a specialized set-up. Industry ready-to-use devices are inflexible in accessing to their components which probably makes their application for ITER extremely difficult.

In the second task a review of the spectroscopic diagnostics foreseen in ITER has been done. Monitoring of the erosion in a tokamak is an important issue from a point of view of the device operation and safety. Besides of development of system for its measurements it is also important to investigate if in the present ITER design any systems which would be helpful for the same purpose. As the candidate method the spectroscopy has been suggested due to its capability to measure the radiation of particles eroded from the wall. The goal of this task was to review the spectroscopic systems foreseen for ITER in terms of their usability for monitoring the erosion in the main chamber and divertor zones. To reach this goal the following problems should be solved:

- specification of the spectral range of a spectrometer to observe the lines which may be useful to characterize influxes of materials eroded from the wall
- establishment of the candidate systems present in ITER design which would be suitable for observation of the demanded lines,
- assessment of the efficacy of the methods for quantitative erosion measurements.

To monitor the erosion of the divertor and main wall spectral lines of carbon, tungsten and beryllium should be under observation. Together with them, it may be also useful to observe spectral lines of hydrogen isotopes. The study describes the choice of lines which may be most convenient for such observations together with specification of the diagnostics which could be applied in this purpose.

Unfortunately an important conclusion is also that the dependence between the impurity influx and spectroscopic data is complex enough to make drawing any estimation on the erosion in dependence of measured spectra extremely difficult. The disadvantages of the method which amplify the difficulties are its incapability to measure the erosion due to non-local deposition, prompt redeposition and melting/brittle destruction. Based on this, it is possible to conclude that the spectroscopic diagnostics cannot be used as the only diagnostics for erosion measurements; however; it can be implemented as an auxiliary system for monitoring erosion phenomena especially in regions which erosion processes are more isolated i.e. main wall.

The study in the framework of the last task was based mainly on the recent results as well as on previous results obtained at IPPLM and other labs and described in the literature. In general, the study leads to conclusion that removal/mobilization is easy to be obtained with the use of laser irradiation, both for thick or thin deposits, but still optimization of the process in regard of application is needed and must be performed carefully with special consideration for the properties of materials which are to be removed. In the case of application of the Nd:YAG laser, regardless on the power density (in the range of parameters of the used system, i.e. ~10^6-10^{10} W/cm^2), the removal is inescapably accompanied by the macroscopic and microscopic dust generation. In these terms the removal of co-deposites (especially those which are thick) can be refereed to removal/mobilization of dust particles. In the experiments the dust was collected by the means of various type of collectors (aluminum cylinders, glass plates, special nets for TEM measurements) and thoroughly analyzed which confirmed that it still contains some amounts of fuel.

The application of the solution in ITER is complicated mainly due to the need of application of asophisticated mechanical set-up especially designed for the harsh environment of a thermonuclear reactor. Two possible solutions can be taken under consideration: port plugged set-up and set-up on a remote handling system.

The first one may be designed in two possible configurations:

- the laser beam can be directed by movable/rotating mirrors which allows to scan the laser beam over the areas which may have deposited hot dust particles. In this case the dust particles are released from surface (in form of ablated material in the case of carbon or metallic droplets in the case of Tungsten or Beryllium) and fall down in case of vertical surfaces or are deposited in closes or further vicinity of the laser interaction area. This phenomena enforces the need of application of the dust collectors (possible in form of a specialized vacuum cleaner or an electrostatic collector) which cannot be integrated with a port-plugged system. There is a

possibility of application of such a collector on the remote handling system and integrating it with a port plug laser head, but in this case integrating of both laser head and dust collector on the one remote handling system seems to be more reasonable.

- In order to move the hot dust from hot zones to cold zones laser-induced shock wave can be used; however; it requires some pressure in the vessel. The surface needs to be irradiated with a significant incident angle ($\leq 60°$). Then the irradiation of the all the surface will require the use of several port plugs (around 8) to have a good coverage of the surface vessel.

The remotely handled solution can be developed by designing an integrated device which can consist of a laser head (or just a laser light delivering system ended with light guiding optics) and a dust collector. In this system the crucial issue is a possibility of the design of an appropriate system of delivering of optical pulses of a given pulse parameters and at given wavelength. Another important issue is the design of the light collecting device. This problems are in scope of the another task of this program.

Spectroscopic and ion diagnostics for laser-induced removal of fuel and co-deposits from PFCs in tokamaks

Corresponding author **Monika Kubkowska**
monika.kubkowska@ipplm.pl

The research conducted in the framework of this project in 2010 included numerous tasks under contracts with EFDA-PWI and JET-FT. The tasks were aimed at various issues consistently covering the area of fuel removal, dust production, first wall erosion and diagnostics for these concomitant phenomena.

Development of the laser removal methods as well as the suitable diagnostics to evaluate their performance has been in the scope of the works at Division of Laser Plasma which fruited in optimization of the method based on the application of Nd:YAG pulse laser for carbon based material and components, development of the LIBS method for the real time characterization of removal and wall composition, application of the LIBS diagnostics for mixed-material analysis or extensive material investigation of the laser treated components and surfaces in collaborating labs.

The experimental set-up has been upgraded and completed in 2010 what is shown in fig. 1. In comparison with the previous years set-ups, the vacuum chamber was equipped with two microvalves which allowed to conduct experiments in ambient of gases and their mixes. In this part of the research, the experiments were conducted in the atmospheres of H_2, N_2, O_2, Ar and their mixes in pressures range from 100 Pa – 100 hPa.

A number of calibrated samples with different mixes of ITER relevant materials have been investigated with the use of LIBS in the same set-up as for the AUG samples. In frame of the project the series of experiments performed in close collaboration with CIEMAT have been done. They were aimed on investigation of the influence of the application of various gasses on the process of laser removal of thick co-deposit from a TEXTOR limiter sample. As concomitant aims the investigation of the influence of the fiber-laser irradiation on the fuel inventory and behavior of dust during the laser interaction should be highlighted.

In all experimental series the removal rate during laser irradiation was positively correlated with the increase of the gas pressure as well as in all cases the process of removal needed less Nd:YAG laser pulses when the Yb:fiber laser had been used for pre-irradiation.

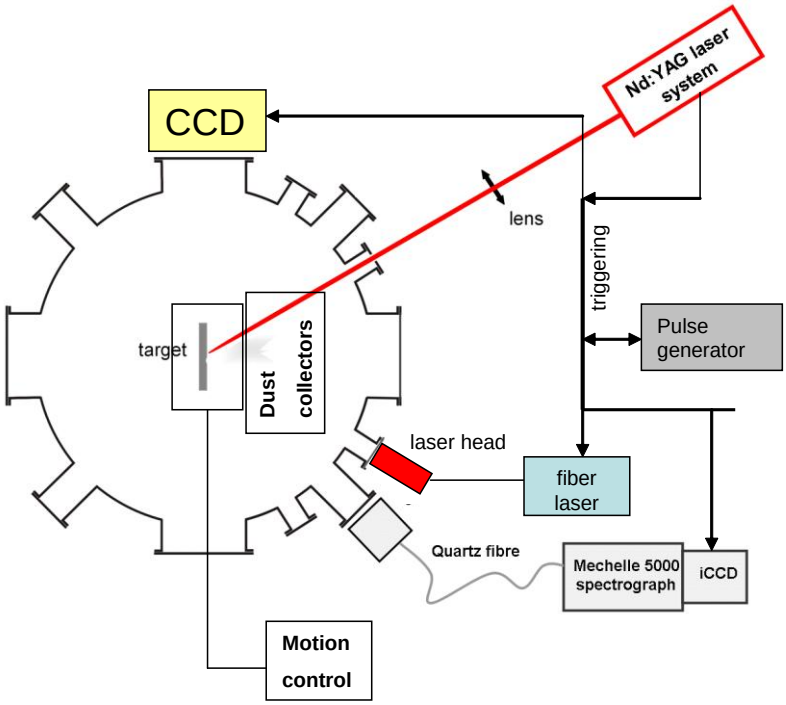

Fig. 1 Upgraded experimental set-up for PWI measurements

For the vacuum conditions, the comparison of the process of removal preceded or not by the fiber laser treatment illustrated as spectral changes corresponding to subsequent pulses of Nd:YAG laser is shown in fig. 2. It can be clearly seen that in the case of fiber-laser pre-irradiation the level of the ratio of the intensities of deuterium and carbon lines (D/C) started from a significantly lower level than in the case when the virgin co-deposit layer was irradiated. As during the Yb:fiber laser pre-irradiation no dust particles were observed it suggests that a significant part of fuel inventory was released during this process by the means of desorption. In case of the removal in vacuum it was also noted that the D/C ratio after five Nd:YAG laser shots was also notably lower in the case when the pre-irradiation were applied.

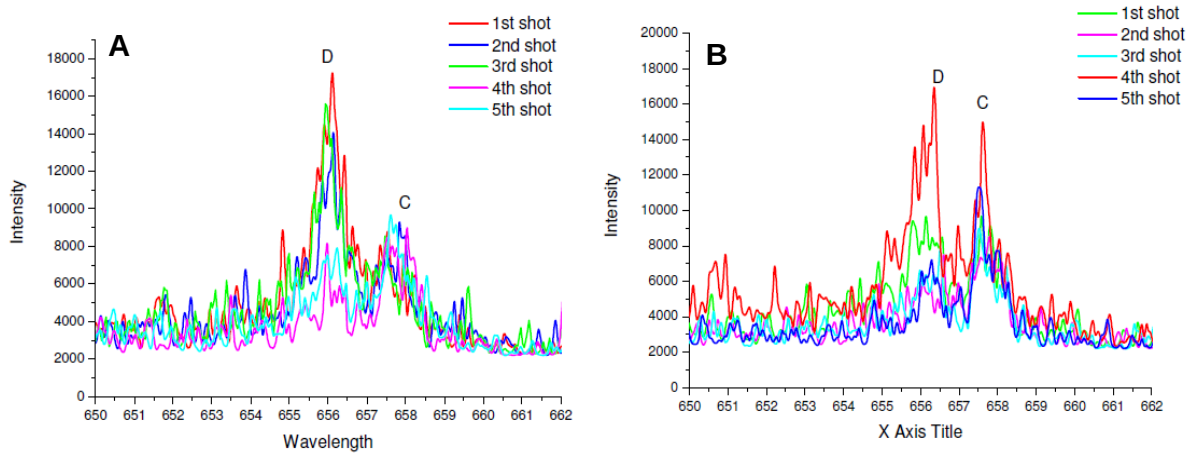

Fig. 2 Comparison of the spectra obtained in vacuum for 5 subsequent laser pulses without (A) and with (B) fiber laser pre-irradiation

Together with LIBS investigation the CCD camera observation has been carried on for the same experimental series. As it has been found in previous experiments the observable dust was being

released 40 μs after the laser impact. The velocity of dust particles was estimated in range of 100 m/s in vacuum and it was decreasing with mass and pressure of the gas when it was applied. Moreover, after the image processing and zooming of the dust traces, the "comet" effect for the high pressure of active gases became apparent which suggested that dust particles were "burning" during their flight. Especially for higher pressures artifacts of long-living plasma even after 100 μs were seen (fig.3).

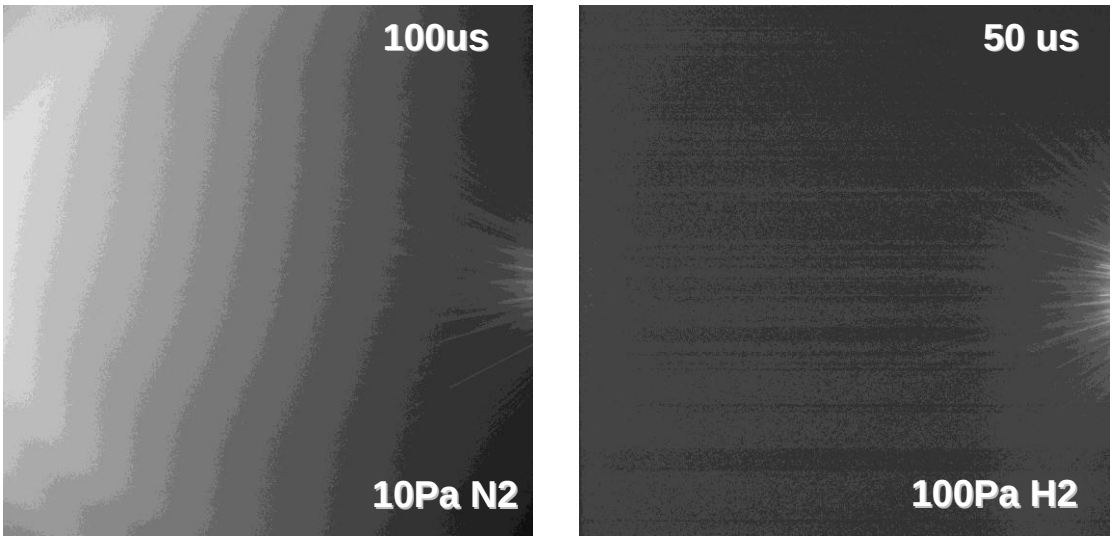

Fig. 3 Images from CCD taken in different experimental conditions with the use of TEXTOR limiter sample (located on the right side of the images). Both images were taken 40 μs after laser pulse

The results obtained in 2010 suggest that the works in this field should be continued with focus at mixed material and optimization of the fiber-laser operation. In the upcoming year the research will be upgraded by the application of a new profilometer system which was purchased in the end of 2010 and will be especially for the characterization of laser induced craters and tracks.

Studies of material erosion and re-deposition on plasma facing components from the present day machines. Characterization of exposed PFCs with various microscopic and analytical techniques (TEXTOR and AUG)

Corresponding author **Elżbieta Fortuna-Zaleśna**
efortuna@inmat.pw.edu.pl

The investigations carried in 2010 included:

- Dust generation in present devices
    - Characterization of dust collected in EU machines (AUG and TEXTOR): TEM, SEM, XPS, AES, BET etc with the special emphasis on size, morphology, composition and internal structure of dust particles

      Fine particles on the surface of the large dust particles (over 50 microns), collected in 2005 and 2007 from ASDEX Upgrade and in 2008 from TEXTOR, were examined by high resolution scanning electron microscopy (HRSEM) and Auger electron spectroscopy (AES).
      In the case of AUG dust tungsten particles were of special interest. Based on the chemical composition, the following types of fine particles were identified: (a) W and W-Al based, (b) Fe based, (c) Ti and Ti-Al based, (d) C based, (e) Si-Al-O based and (f) Ag based.

In the case of TEXTOR dust, the particles were primarily metallic (iron, chromium and nickel rich) with a large number of carbon rich flakes. Ceramic particles containing Si, Al, O were also detected.

- Characterization of the dust samples from AUG: plasma produced dust, captured by filtered vacuum collection with Teflon membranes of 1 micron pore size

  The detailed characterization of the morphology of tungsten particles from the dust probe S08 collected after 2009 campaign has been carried out using HRSEM. Their composition was examined by EDS.

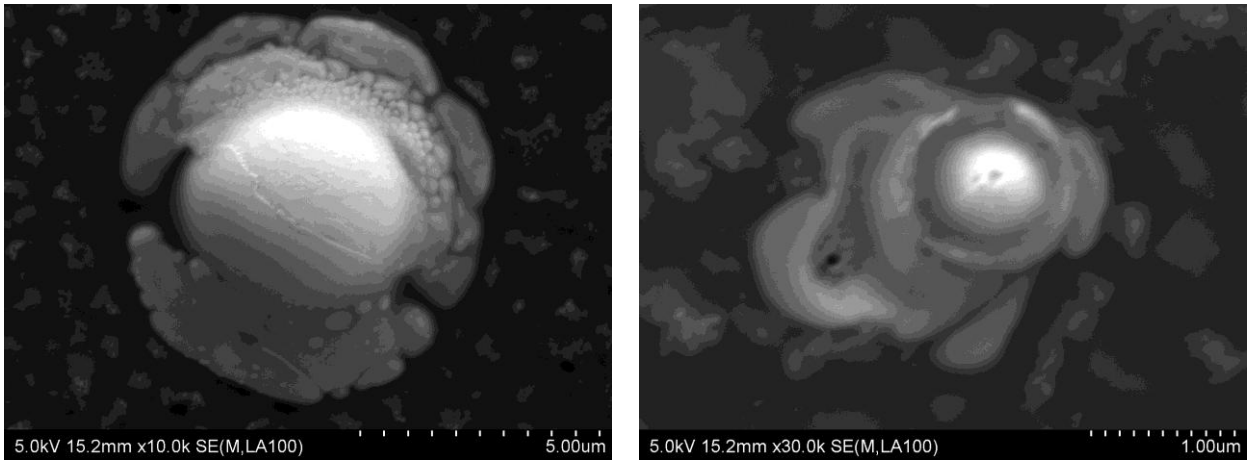

a) b)

Fig. 1 Images of the round tungsten particles embedded into material of different chemical composition

Characterization of AUG divertor outer strike point tiles with various microscopic and analytical techniques (TEM, FIB, SEM, XRD, AES etc)

The present investigations were carried out on 13 samples from outer divertor Tile 1 of ASDEX Upgrade, with s coordinates from 1038 to 1231 mm. This tile was installed in the machine for one 2009 campaign, during which three boronizations took place. The samples differed in received flux, which can be specified based on the s-coordinates. The tile was coated with a 10 µm W layer deposited on fine grain graphite with a 2-3 µm Mo interlayer. The aim of these post-mortem examinations was material mixing and description of plasma-induced damage of tungsten coatings.

It has been generally observed that the surface morphology of the tungsten coating after the exposure shows a directional character of erosion and deposition. The deposits form mostly in the shadowed areas. Their thickness, according to FIB/STEM examinations varies from 200 nm to 1.5 µm, depending on the sample location and amount of received flux. The investigations revealed mostly W and W/O deposits. The structure of the re-deposited tungsten is highly porous and resembles a foam or sponge.The XPS and AES examinations confirmed that the main constituents of the deposits are tungsten (40-60 at.%), oxygen (15-40at.%) and carbon (15-20at.%). Residues of iron were also observed. The amount and morphology of the boron deposition varied strongly with the position of the sample.

The roughness measurements confirmed surface smoothening caused by erosion.

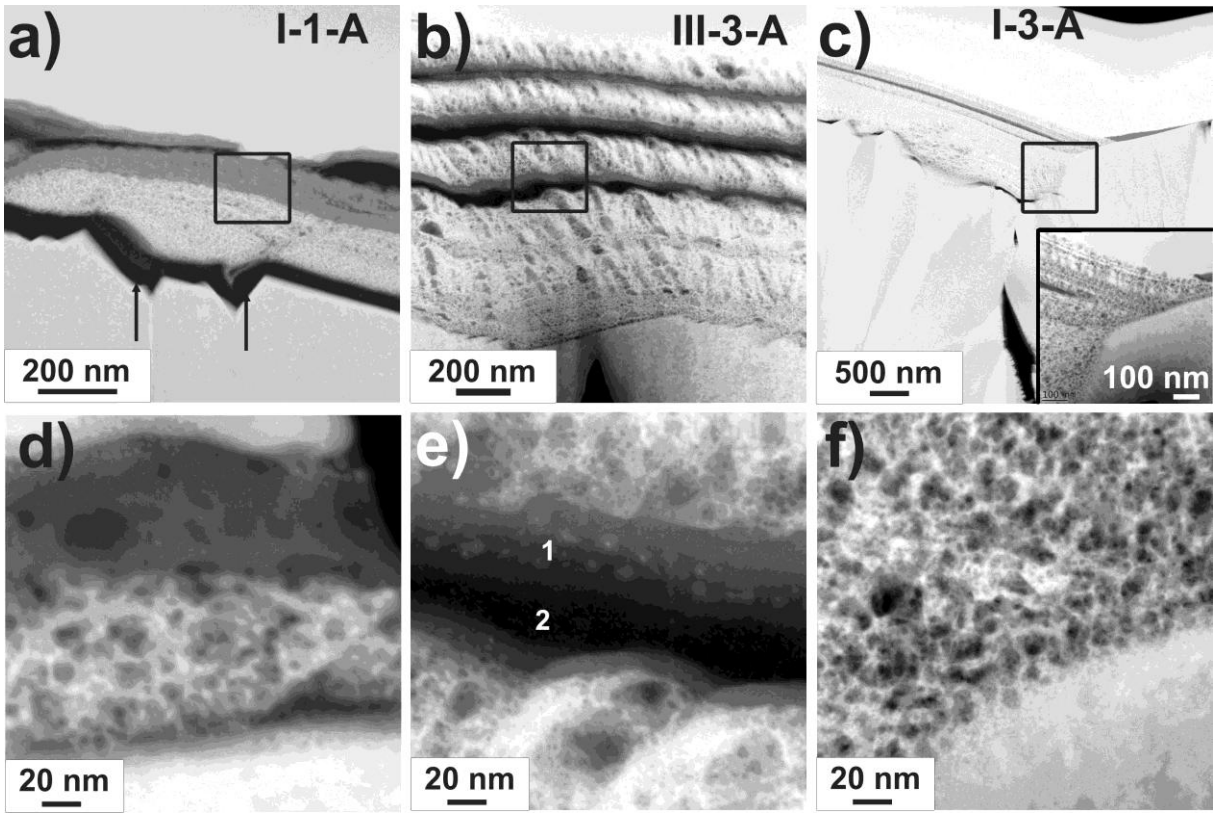

Fig. 2 STEM Z-contrast images representing cross-sections of eroded and deposited layers

PWI in a full W device

Two types of tungsten has been investigated: ITER grade and MF reference. The materials have been provided in two un-implanted states i.e. recrystallized at 2000K and outgassed at 1200K. Those have been studied before and after implantation. The un-implanted ITER grade recrystallized material has been used to prepare a defect-free TEM lamella. To this end two lamella preparation routes were employed. First one used Focused Ion Beam (FIB) milling followed by low energy ion milling aimed at removal of FIB introduced structural damage. The second one was "standard" TEM preparation consisting of mechanical cutting, grinding and dimpling followed by electrochemical polishing. Also multiple process parameters were used for FIB and gentle milling preparation no satisfactory result has been obtained. Only the "standard" preparation route yielded the lamellae without sample preparation introduced damage.

Four implanted materials have been examined: 1) MF reference outgassed at 1200K, 2) MF reference recrystallized at 2000K, 3) ITER-grade outgassed at 1200K and 4) ITER-grade recrystallized at 2000K. All the samples have been subjected to D implantation with a dose of $2e^{25}$ D/m^2 with energy of 25eV/D at 500K. Theses samples have been used to prepare TEM lamellae using the standard preparation route.

No evidence of structural damage after D implantation has been observed in the ITER-grade recrystallized samples. The dislocation structures observed shall be attributed to post-implantation mechanical damage of the specimens. In the outgassed materials the dislocation density was much higher than for the recrystallized ones, as expected. The TEM investigations have shown smudged contrast around dislocation lines that may be attributed to decoration of dislocation by D ions. Also disturbance of atomic lattice of W was observed that might be attributed to implantation damage. Further studies involving in-situ TEM heating experiments have been performed to substantiate these. O change was however observed when heating up to 500°C. Therefore, it should be concluded that no evidence of W damage due to performed D implantation has been observed.

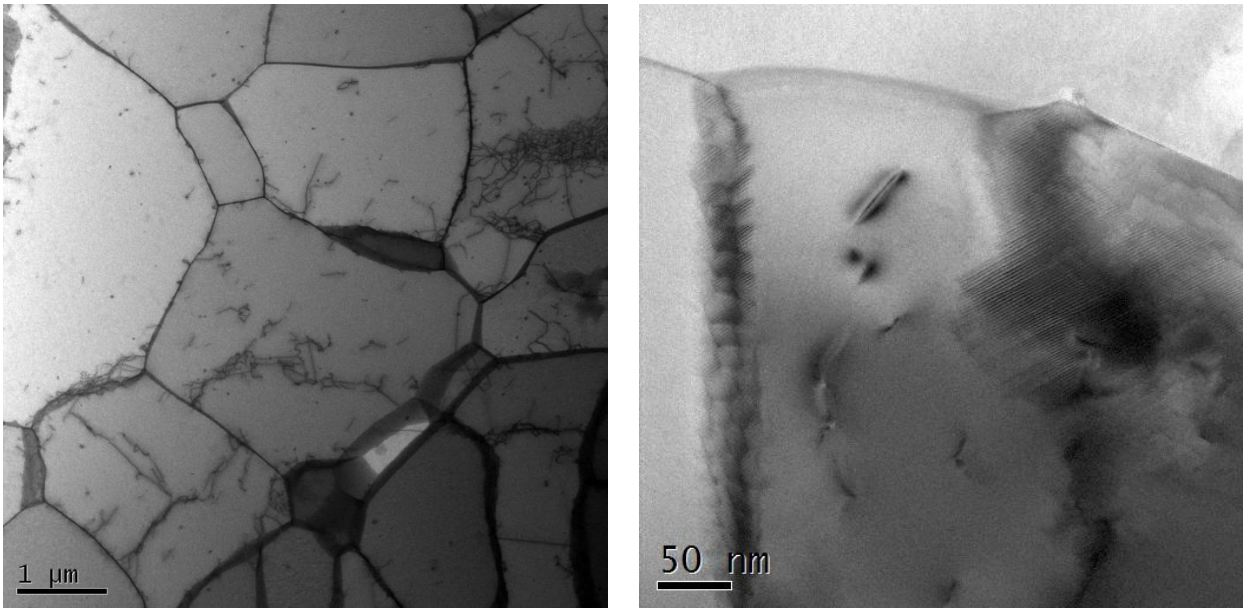

Fig. 3 TEM images of MF reference sample, recrystallized at 2000 K subjected to D ion implantation

3.3 Development of material science and advanced materials for DEMO

Ab-initio study of defects configurations and their interactions in W-Ta and W-V model alloys

Corresponding author **Łukasz Ciupiński**
lukas@inmat.pw.edu.pl

The structure and phase stability of binary tungsten-vanadium and tungsten-tantalum alloys are investigated over a broad range of alloy compositions using *ab initio* and cluster expansion methods. The alloys are characterized by the negative enthalpy of mixing across the entire composition range. Complex intermetallic compounds are predicted by *ab initio* calculations as the low temperature ground states for both alloys. The effect of atomic relaxation on the enthalpy of mixing is almost negligible in W-V, but is substantial in W-Ta alloys. Canonical Monte-Carlo simulations are used for evaluating the order-disorder transition temperatures for both alloys. Differences in the short-range order characterizing the alloys are explained by the opposite signs of the second nearest-neighbour cluster interaction coefficient for W-V and W-Ta. Using the predicted ground-state structures, we evaluate the mono-vacancy formation energies and show that in W-Ta alloys they are highly sensitive to the alloy composition and to the local environment of a vacancy site, varying from 3 to 5 eV. A <111> self-interstitial atom crowdion defect in tungsten forms a configuration strongly bound to a vanadium solute atom, whereas interaction between the same defect and a tantalum solute atom is repulsive. Values of elastic constants computed for all the ground states and several meta-stable cubic alloy structures are used for assessing the effect of alloying on mechanical properties. Values of the Young modulus and the Poisson ratio, as well as the empirical Rice-Thompson criterion, are applied to screening the alloys, to assess the effect of chemical composition on ductility.

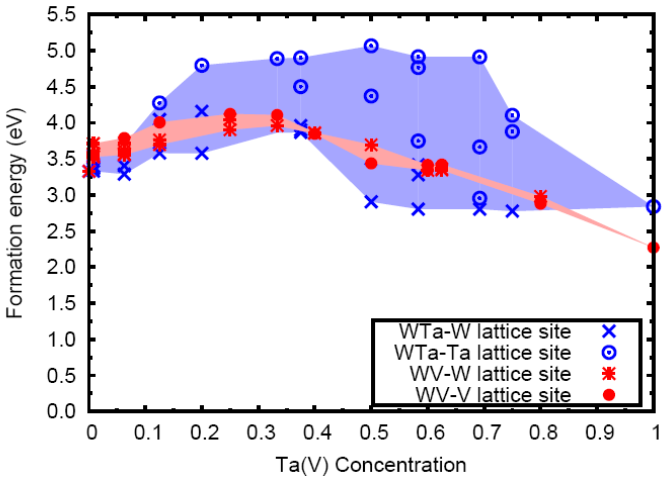

Fig. 1. Mono-vacancy formation energies computed for the ground state intermetallic structures of W-Ta and W-V binary alloys

W/steel joints fabrication route based on pulse plasma sintering (PPS) method and explosive bonding

Corresponding author **Łukasz Ciupiński**
lukas@inmat.pw.edu.pl

Tungsten-to-steel joints development by PPS method

Series of tungsten/steel joints with different interlayers were produced by PPS. For this purpose, disks 12 mm in diameter and 3 mm thick were cut from the as-received Eurofer 97 steel and tungsten rods, which were subjected to sintering by the PPS method with 1 mm thick interlayers. The interlayers used were: 25wt.%Fe-Ti, 86wt.%Fe-Ti and pure Fe. The quality of the joints was verified by SEM investigations of cross-sections. The phase compositions were determined by XRD. The joint with 25FeTi interlayer was rejected, because of its brittleness.

The most promising joints, namely W/86FeTi/Eurofer 97 and W/Fe/Eurofer 97, were selected for thermal shock tests. Thermocycle tests of the sintered W/Eurofer 97 joints were performed to evaluate the durability and reliability of the joints. Five samples of each type of the joint were subjected to heating to 700°C for 15min in an Ar atmosphere, maintaining for 2min, and quenching in water. After each cycle the samples were examined for possible cracks or delamination. The joints with the Fe interlayer appeared to be more resistant to the shocks.

Moreover, attempts were made at direct welding of tungsten and its alloy (WL10). Welding processes were carried out at 1000, 1100 and 1200°C for 30min. The microstructure of the joints thus produced was characterized. The quality of the joints fabricated at 1100°C and 1200°C is good.

Finally, the experiments of welding tungsten alloy and steel components of complex geometry were carried out. The welding process was conducted at 700°C for 30min. and an iron foil was used as interlayer. The results of microstructure investigations of the joints produced indicate suitability of the PPS method for the complex geometry joints development and use of Fe as technological interlayer.

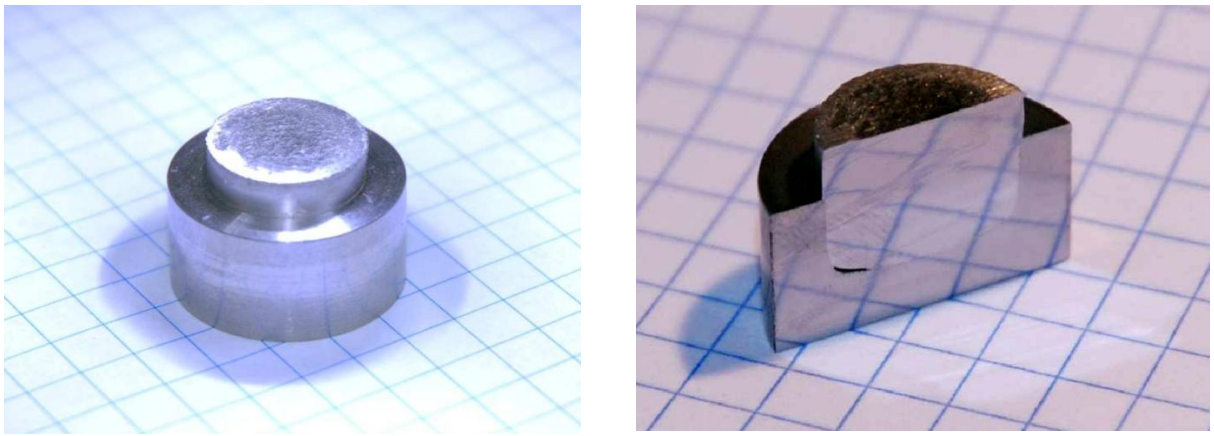

Fig. 1 Macroscopic images of a welded WL10/Eurofer 97 joint

Tungsten-to-steel joints development by explosive bonding

The objective of the task was to assess the feasibility of fabricating the W-to-steel joints using explosive bonding. To this end preliminary experiments of bonding two steel plates were performed. In these experiments hard and low ductility steel (BRINAR 500) was bonded to soft steel in order to evaluate the initial parameter range for W-to-steel joining. Furthermore, the trials have been performed with as setup allowing for quick heating of tungsten plate before detonation. Finally, based on the results of these preliminary tests, a setup of inversed geometry and a technological interlayer of soft material was prepared for W-to-steel joining experiments.
The explosion bonding of W-to-steel was performed using 10mm thick low alloy steel plate as a flayer plate, 2 mm thick electrolytic Cu99,9E copper sheet as the technological interlayer and 2 mm thick tungsten sheet form PLANSEE. The obtained joint was characterized using SEM and optical microscopes, microhardness measurements and bending tests in 3 perpendicular directions.
It has been shown that due to the high brittleness of tungsten the cracks develop in the tungsten cladding in the majority of the clad area. However, a crack free region exists at the first 10% of the joint length along the detonation wave direction.

The microstructural observation revealed oxidation of the Cu interlayer at the Cu/W interface. The joint of flat geometry was observed with generally good adhesion. Microhardness measurements revealed increase of the hardness of both joined materials (Cu and W) in the vicinity of the “fusion” line. Finally, the bending tests resulted in internal delamination of tungsten cladding that occurred in the cladding itself, i.e. the remnants of tungsten were always observed on the Cu interlayer, suggesting good adhesion of tungsten to copper.

The results obtained allow to conclude that fabrication of W to steel joints by explosive bonding is feasible, however an interfacial soft material shall be used, due to brittleness of tungsten, and low detonation speed explosives shall be employed. Any means allowing for increased plasticity of tungsten shall be exploited in order to facilitate the joint development by explosive bonding.

Fig. 2 Tungsten-to-steel joints produced by explosive bonding after bending tests

Hydrostatic Extrusion (HE) processing of ODS ferritic steel: microstructure characterisation, mechanical properties and thermal stability

Corresponding author **Małgorzata Lewandowska**
malew@inmat.pw.edu.pl

Two oxide dispersion strengthened ferritic steels were produced by means of mechanical alloying followed by HIPping. Mechanical alloying process of a pre-alloyed Fe-14Cr-2W-0.2Ti ODS powder was performed using 0.5% Fe_2Y intermetallic compound powder and the 0.3% Y_2O_3 particles. The Fe_2Y powder were used to decrease oxygen content of the ODS FS alloy and improve mechanical properties, especially impact fracture, both the upper shelf energy and transition temperature, and to find out whether it is possible to synthesized new thermally stable nanoparticles (nanoclusters).

The results presented in this work have shown that an oxide dispersion strengthening ferritic steel can be manufactured by MA of the Fe_2Y intermetallic compound with pre-alloyed Fe-14Cr-2W-0.2Ti powder by internal dissolution and further precipitation process. Moreover, using the Fe_2Y powder instead of Y_2O_3 powder results in a significant reduction of the oxygen content. This leads to considerable Charpy impact properties improvement with a DBTT of about - 24° C and an USE 8.8 J, in comparison with the ODS Y_2O_3 material which exhibits a very low USE of about 2.4 J and a high DBTT of about 77° C.

TEM observations revealed that the microstructure of both ODS materials is typical for as-HIPped ODS materials and consists of a mixture of the smaller (few hundred of nanometers) and coarser (up to few μm) grains. However, some differences were observed in the size and distribution of the nanoclusters. Larger and less densely distributed nanoparticles were detected for the Fe_2Y ODS material. In addition, annealing process of both ODS materials at 1350°C for 1 h in argon reviled grain growth and nanoparticles coarsening. As expected, more stable microstructure and nanoparticles has the Y_2O_3 ODS alloy, whereas significant nanoparticles coarsening up to 100 nm were measured for the Fe_2Y ODS alloy. Also, interestingly it appears that these coarser nanoparticles in the Fe_2Y ODS steel after annealing at 1350°C have an austenitic γ-fcc structure.

Thus, using intermetallic Fe_2Y powder instead of Y_2O_3 particles can be an effective approach for producing a material with improved impact properties. However, the thermal stability, creep and irradiation behaviour of the ODS steels are also important parameters which should be examined.

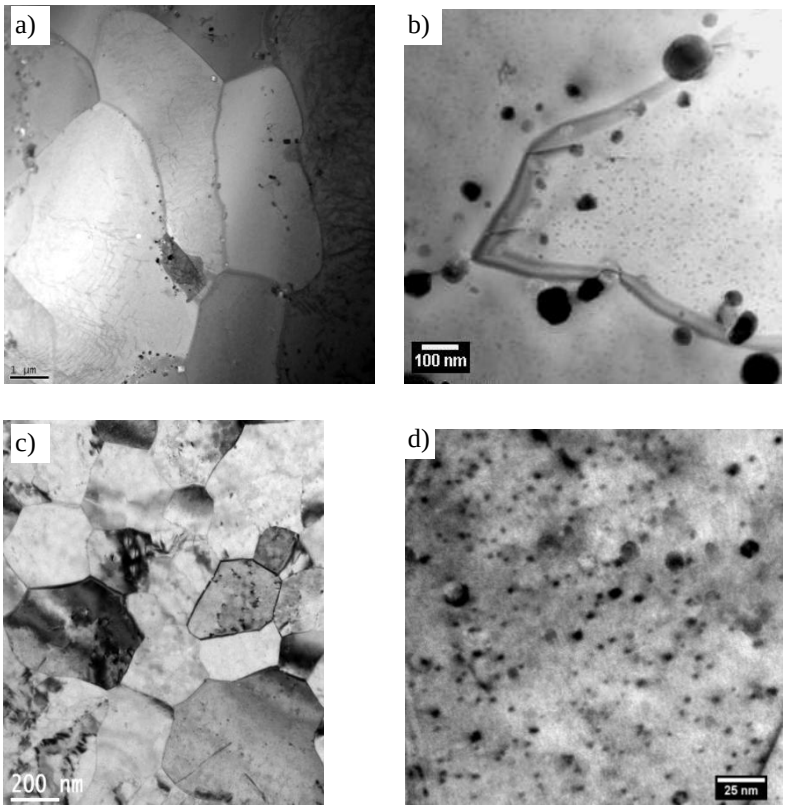

Fig. 1 TEM images of the microstructure of the ODS steels after HIPping and HT at 1350°C:
a) Fe_2Y ODS, general view, b) Fe_2Y ODS nanoclusters, c) Y_2O_3 ODS, general view and d) Y_2O_3 ODS nanoclusters

Application of Mössbauer spectroscopy to Fe alloys characterization

Corresponding author **Stanisław M. Dubiel**
dubiel@novell.ftj.agh.edu.pl

A series of $Fe_{100-x}Cr_x$ alloys with $x \leq 25$, including three EFDA model alloys, was investigated using Mössbauer spectroscopy (MS). The study was aimed at (1) determining an atomic short-range order (SRO), and (2) the Debye temperature, Θ_D. Concerning (1) a distribution of Cr atoms within the first two coordination shells, *1NN-2NN*, around probe ^{57}Fe atoms was determined from the spectra recorded at 295 K. A clear evidence was found that the distribution is not random but characteristic of a given atomic configuration, *(m,n)* (*m* being a number of Cr atoms in *1NN*, and *n* that in *2NN*). The behavior was described quantitatively in terms of a local SRO-parameter, $\alpha(m,n)$, for each *(m,n)* as well as in terms of average SRO parameters, $<\alpha_1>$, $<\alpha_2>$ and $<\alpha_{12}>$. The inversion was found both in $<\alpha_1>$ and in $<\alpha_2>$, though going with *x* in opposite directions. The behavior resulted in a lack of the inversion in $<\alpha_{12}>$. The latter was positive indicating the atomic short-range order.

The Debye temperature was evaluated from the temperature dependence of the centre shift of the Mössbauer spectra measured in the temperature range of 60 – 300 K. Its compositional dependence shows a non-monotonous behavior with two peaks: a sharp maximum at $x \approx 3$ having a relative increase of ~10% compared to a pure iron, and a broad one centered at $x \approx 15$ with a relative height of ~12%. The positions of the peaks correlates quite well with those found or calculated for various physical properties like the spin-waves stiffness coefficient, D_o, the magnetic moment per Fe atom, μ, and the Curie temperature, T_C, suggesting a magnetic origin as a possible source of the anomalous behavior of Θ_D observed in this study.

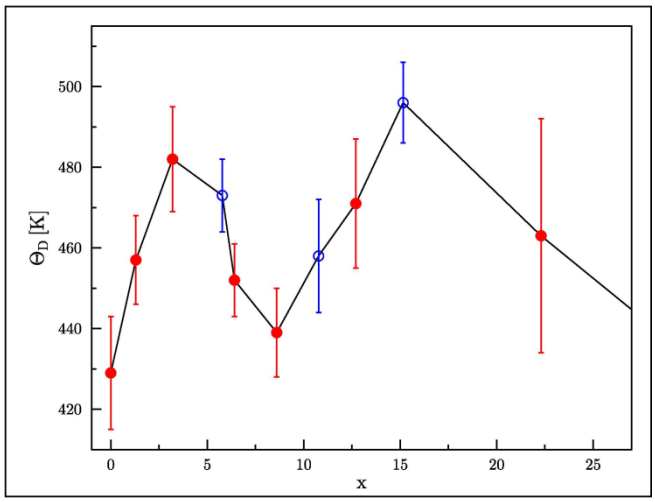

Fig. 1 Debye temperature, ΘD, versus chromium content, x.
The model EFDA samples are indicated by open symbols. The solid line is a guide to the eyes

Mathematical modelling of thermal-hydraulic problems related to the HTS

Corresponding author **Monika Lewandowska**
mlewandowska@zut.edu.pl

Previous tests results have revealed that the use of HTS current leads (CL) for ITER would provide considerable savings in the refrigeration operation costs with respect to the conventional metallic current leads. Further development of this promising technology would be advantageous. The work focused on preparation for experimental tests of HTS CL at the EPFL-CRPP (PSI Villigen), which was the key activity undertaken in the reporting period. Other activities were aimed at completion of investigations which had been carried out in 2008-2009.
The experimental investigations of HTS CL is foreseen at the EPFL- CRPP (PSI Villigen), which requires extending the capabilities of the existing JORDI facility in order to perform tests of HTS CL's in different cooling conditions. The conceptual design of the cryogenics needed for the facility upgrade considering the requirement of as extended as possible range of operation was developed. In particular, we considered: (i) a variable helium mass flow rate at low temperature (4.5 K) to obtain the required mass flow rate of 50 K helium from the mixing of the existing low temperature and room temperature lines, (ii) two cooling options for the copper part of a CL, (iii) the use and sizing of heat exchangers in the cryogenic circuit. It results from our analysis that the proposed cryogenic circuit is capable to provide sufficient amount of coolant needed to perform tests of HTS CL's in the most demanding planned conditions.

Two final-design ITER TF dual channel CICCs were tested in the SULTAN facility in 2008-2009. The samples were heated either by eddy current losses induced in the strands by an applied AC magnetic field or by foil heaters mounted on the outside of the conductor jacket. In the reported period, the steady-state temperature response of several thermometers installed on the jacket surface as well as inside the cable were analyzed, using the two-channel analytical model proposed by Renard et al., to obtain the equivalent transverse heat transfer coefficient between the bundle and central channel. In addition, on the basis of the measured pressure drop and helium flow velocities, the friction factors for helium flow in bundle and central channel were obtained as a function of the mass flow rate. The results of these investigations were presented in: Lewandowska M., Herzog R.: Transverse heat transfer coefficient in the dual channel ITER TF CICC's. Analysis of the steady state temperature profiles resulting from the annular heating. Submitted for publication in Cryogenics.

The last activity carried out in the reporting period was the completion of the cool-down analysis of the European EDIPO test facility. The thermo-hydraulic analysis of the EDIPO cool-down was performed in order to assess its duration for two possible schemes of the cooling circuit in the EDIPO windings (coils connected in series and coils connected in parallel). It was assumed that EDIPO would be cooled by helium flowing in the windings and in the outer cooling channel connected in parallel. We took into account limitations due to: (i) the acceptable level of thermal stress, (ii) the pressure drop in the cooling circuit, (iii) the refrigerator capacity. The initial cool-down analysis was performed in 2009 using the simplified analytical model, which neglected the delay due to the heat conduction in the EDIPO main body. In the reported period, the analytical model was complemented by a new numerical model of the heat conduction in the EDIPO main body. In the numerical model the EDIPO main body was assumed to be a 2D axially symmetric object with orthotropic, temperature dependent material properties. We took into account heat transfer between the EDIPO main body and the windings and from the EDIPO main body to helium in the outer cooling channel. The final results of this analysis were presented in: Lewandowska M., Bagnasco M., Thermo-hydraulic analysis of the cool-down of the EDIPO test facility. Submitted for publication in Cryogenics.

3.4 Fusion plasma diagnostics

Activation technique in a cross-check experiment for high resolution neutron spectrometry

Corresponding author **Marek Scholz**
marek.scholz@ipplm.pl

The activation method is commonly used (mainly in fission reactors and accelerator-driven generators) to determine neutron fluence or energy spectrum. It is basing on recovering the information about neutrons by registering the products of induced reactions.

As the detectors there are used the samples of selected materials. In those samples irradiated in neutron field there are induced reactions creating radioactive nuclei. The chosen materials have relatively high cross-section for reaction with neutrons in specified energy range. The reactions are chosen in such way that they products decay with emission of gamma-ray. Therefore they can be detected by means of gamma-spectrometry.

For every registered reaction there is calculated reaction rate:

$$\alpha_i = \int_0^\infty \sigma_i(E) \cdot \varphi(E) \cdot dE \qquad i = 1, \ldots, n \qquad (R1)$$

where $\sigma_i(E)$ – i-th reaction cross-section, $\phi(E)$ – neutron flux density, E – incident energy, n – quantity of reactions.

The set on n degenerate equations (R1), which are a special form of Fredholm integral equations, makes ill-conditioned problem, i.e. it does not allow to unique determine neutron flux or spectrum because there is infinity number of $\phi(E)$ functions which satisfy the set of equations (R1) but only one of them is physical correct. It causes that such problem should be solved by means of approximate (numerical) methods. In general such kind of equations is solvable in discrete form and leads to the set of n linear equations:

$$\alpha_i = \sum_{j=1}^{m} \sigma_{i,j} \cdot \varphi_j \qquad i = 1,\ldots,n \qquad (R2)$$

where m is the number of energy bins (groups), $\sigma_{i,j}$ – mean value of i-th reaction cross-section in j-th energy bin, ϕ_j – mean value of neutron flux density in j-th energy bin.

To determine neutron spectrum in n energy ranges by means of activation method there should be registered n nuclear reactions (and therefore n reaction rates). It is not possible to obtain accurate solution for more than n ranges. Usually the number of energy bins needed to precise description of the spectrum is greater than the number of registered reactions (m > n). It causes that the problem is not solvable without providing some additional information about demanded spectrum being it the best available approximation. This information arise usually from physics of investigated phenomenon or from neutron transport calculations, e.g. by means of MCNP code. Deconvolution algorithms are used to modify such initial information until obtain compatibility with experimental data.

The method is basing on recovering the information about neutrons by registering the products of induced reactions. As the detectors there are used the samples of selected materials. In those samples irradiated in neutron field there are induced reactions creating radioactive nuclei. The chosen materials have relatively high cross-section for reaction with neutrons in specified energy range. The reactions are selected in such way that they products decay with emission of gamma-ray, therefore they can be detected by means of gamma-spectrometry. Exceptionally, there are also used reactions leading to beta-radiation.

Additionally, materials of the samples can to be chosen in such a way, that neutrons with energies of 14.1 and 2.45 MeV and scattered neutrons can be measured separately.

The uncertainty depends mainly on the accuracy in the cross sections and in the geometry factor. It is acknowledge that the yield of the 2.45 MeV neutrons can be determined with an accuracy less than 10%.

Selection of the activation materials

Apart from indium which is particularly well suited as an activation detector for plasma devices, also other materials are needed. Developing the activation method of neutron measurements at JET we are still searching for suitable activation materials

To carry out the activation measurements at JET there were selected the reactions which meet the requirements of measuring procedure.

It means that isotopes naturally occurring in activation materials must have high enough reaction cross-section in relevant neutron energy range. At the same time, the products of these reactions should decay with appropriate half-live and emit suitable gamma-photons.

The neutrons at JET come from d-d fusion and in small part from tritium burn-up. Originally they are 2.45 and 14.1 MeV in energy respectively which is broadening by reason of plasma temperature and applied heating systems. The plasma pulse at JET takes usually about 0.5 minute, whereas the main neutron emission occurs only during Neutral Beam Injection (NBI) heating which lasts for a few seconds only. Applying procedure demands about 0.5 minute more of time for operation. Therefore there were chosen reactions sensitive to characteristic plasma neutron energies which products decay with half-live counted in more than a few seconds. Because of properties of applying gamma-spectrometer the reaction products must emit during decay gamma-line of energy from 100 keV up to 2000 keV.

During selection there were assumed that the most useful cross-section is counting at least in hundreds of milibarns.

The materials selected in our laboratories have been subjected to numerous of testing measurements.

Table R1

№	Reaction	Threshold [MeV]	Product half-live
1	Ti-47 (n,p) Sc-47	1.8	3.3 d
2	Fe-54 (n,p) Mn-54	1.8	312 d
3	Ni-58 (n,p) Co-58	1.6	71 d
4	Se-77 (n,n') Se-77m	0.2	17 s
5	Br-79 (n,n') Br-79m	0.2	5 s
6	Sr-87 (n,n') Sr-87m	0.4	2.8 h
7	Y-89 (n,n') Y-89m	1.2	15.7 s
8	Zr-90 (n,n') Zr-90m	2.3	0.8 s
9	Cd-111 (n,n') Cd-111m	0.5	49 m
10	In-115 (n,n') In-115m	0.6	4.5 h
11	Er-167 (n,n') Er-167m	0.3	2.2 s
12	Hf-177 (n,n') Hf-177m	1.3	51 m
13	Au-197 (n,n') Au-197m	0.5	7.7 s
14	Pb-207 (n,n') Pb-207m	1.6	0.8 s

Table R2

№	Reaction	Threshold [MeV]	Product half-live
1	Al-27 (n,p) Mg-27	4.3	9.5 m
2	Al-27 (n,α) Na-24	6.8	15 h
3	Ti-46 (n,p) Sc-46	3.8	84 d
4	Ti-48 (n,p) Sc-48	7.4	44 h
5	Fe-56 (n,p) Mn-56	7.0	2.6 h
6	Co-59 (n,α) Mn-56	8.5	2.6 h
7	Co-59 (n,2n) Co-58	10.8	71 d
8	Zn-64 (n,2n) Zn-63	12.6	38.5 m
9	Zr-90 (n,p) Y-90	7.6	3.2 h
10	Zr-90 (n,2n) Zr-89	12.2	4.2 m
11	Nb-93 (n,2n) Nb-92	9.1	10.1 d
12	Mo-92 (n,2n) Mo-91	12.8	15.5 m
13	Au-197 (n,2n) Au-196	8.8	9.6 h
14	Pb-204(n,n')Pb-204m	2.7	67 m

An important part of measurement by activation technique is spectrum unfolding.It is based on measurements of radioactivity induced in samples by neutron fluxes. From mathematical point of view this process is identical as solving Fredholm integral equation of the first kind. Analyses of seven unfolding methods were carried out – least squares method, minuit routine, Tikhonov regularization method, neural networks, genetic algorithm, Gold and SAND-II algorithms. Computer programs were

developed using Gold and SAND-II algorithms. Activation measurement made during shots at JET were used in this process. Results obtained with GOLD were evaluated negatively, it is not the right method for unfolding spectra in the broad energy range (0 – 15 MeV) and several (15-16) activation detectors. Spectra unfolded with the SAND-II algorithm were evaluated better but mainly jagged spectrum below 1 MeV is appeared, due to resonance cross section influence (Fig. 1)

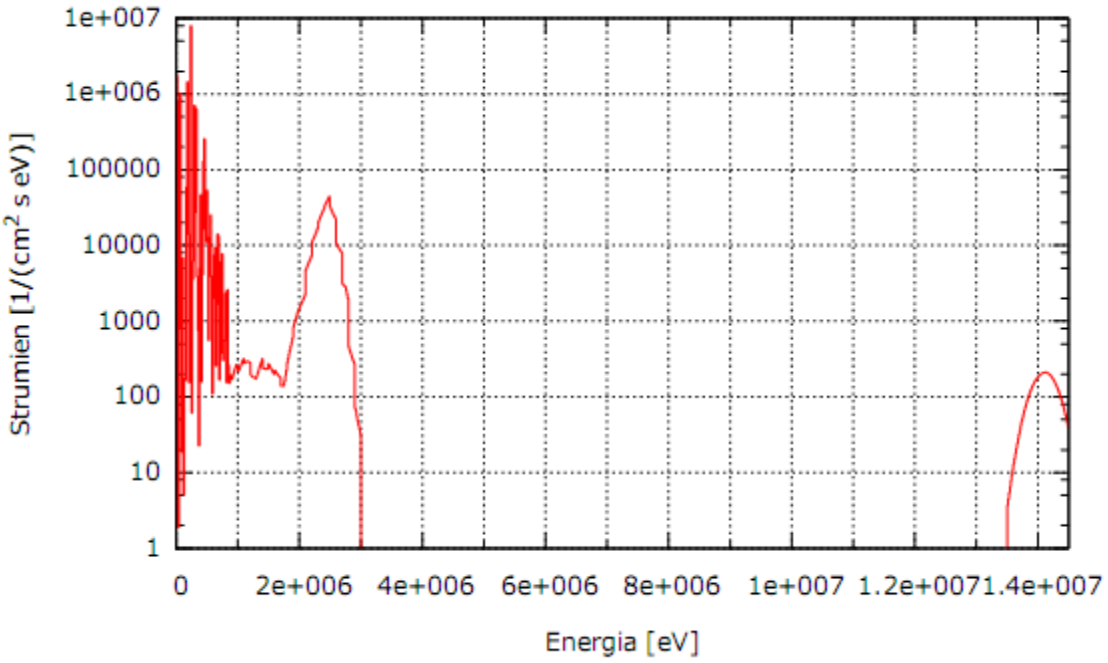

Fig.1 Neutron spectrum for JET shot 78055 unfolded by SAND-II

Diamond detectors to detect escaping fast alpha particles

Corresponding author **Krzysztof Drozdowicz**
krzysztof.drozdowicz@ifj.edu.pl

Fast neutrons and alpha particles will be produced in the fusion reaction in hot deuterium-tritium plasma in future thermonuclear reactors which will be used in power plants. Energy of the created alpha particles should be used to support maintenance of the plasma burning. Thus, it is necessary to measure energy of the alpha particles which escape from the plasma. A study of using diamond detectors for the purpose has been continued.

The energy from nuclear reaction of the alpha particles is 3.5 MeV. Losses of α particles from plasma could extinguish the burn and might induce melting of the first wall. In the previous year a method of precise energy calibration of the diamond detector was elaborated. During that research two isotopic alpha sources and van de Graaff ion beams were used. Finally, a method with use of only one source, AMR33, was proved.

Energy calibrations were made for new bought diamond detectors manufactured by the Diamond Detector Ltd. of a high purity CVD (Chemical Vapour Deposition) single crystal diamonds. The detectors are the same as in the first series and the calibration was performed with the AMR33 source according to the method achieved. Spectrometric detection of protons was tested with mono-energetic beams of protons from the van de Graaf accelerators in the Soltan Institute of Nuclear Studies (Świerk/Otwock, Warsaw Branch) and in the Institute of Nuclear Physics (Krakow). The scattered beam geometry was used. The energy calibration with the protons or alpha particles gave a slightly different results. This effect will be studied in detail in the next stage of the project.

Measurements of the spectrum of the D-T reaction products emitted by a fast neutron generator made

it possible to observe the diamond detector response for the alpha particles in presence of mixed field of other radiations, similarly like it is in tokamaks.

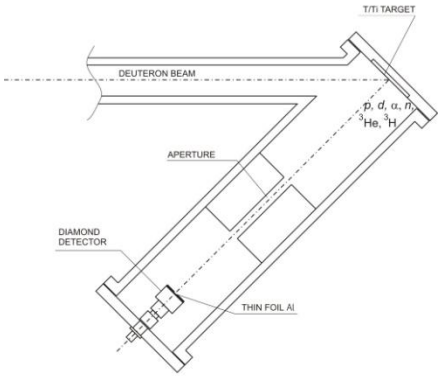

Fig. 1 Geometry of measurement of particles at the neutron generator target.

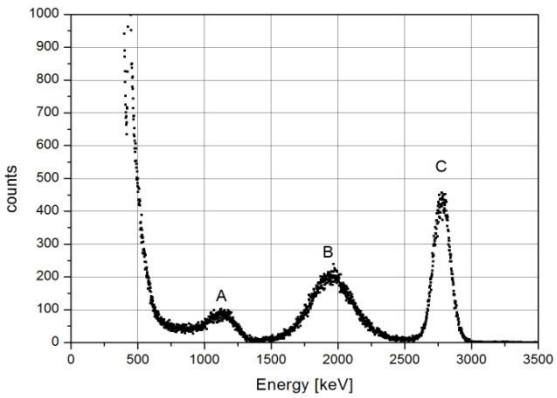

Fig. 2 Spectrum of particles measured at the fast neutron generator.

In the experiment we used a T/Ti target bombarded by the ~100 keV deuteron beam (Fig.1). Some of deuterons penetrate to their maximum range and are retained in the target material at that depth. In this case the neutron generator produces fast neutrons and alpha particles in the reaction:

$$^2D + {}^3T \rightarrow n\ (14.1\ MeV) + {}^4He\ (3.5\ MeV), \qquad Q = 17.6\ MeV \qquad (1)$$

After some time of the use the target contains deuterium implanted from the bombarding ion beam and the following reactions occur:

$$^2D + {}^2D \rightarrow {}^3He\ (0{,}82\ MeV) + n\ (2{,}45\ MeV), \qquad Q = 3{,}27\ MeV \qquad (2)$$

$$^2D + {}^2D \rightarrow {}^3T\ (1{,}01\ MeV) + p\ (3{,}02\ MeV), \qquad Q = 4{,}03\ MeV \qquad (3)$$

Tritium decays to ^3He ($T_{1/2}$ = 12.5 years) and, therefore, some amount of ^3He appears in older targets. ^3He reacts with deuterons and alpha particles (^4He) are emitted:

$$^2D + {}^3He \rightarrow {}^4He + p, \qquad Q = 18{,}3\ MeV \qquad (4)$$

All reaction products, Eqs (1) – (4), emitted from the target and the backscattered deuterons reach the diamond detector shielded with a thin aluminium foil (1.5 mg/cm^2) to avoid gathering an electrical charge. The energy spectrum of the particles created in the fast neutron generator is shown in Fig. 2. Energy of the alpha particles from reaction (1) emitted at 135º is 1.89 MeV. Protons from reaction (3) have energy of 2.7 MeV. Alpha particles associated with reaction (4) have 1.92 MeV. In the spectrum, peak B is, in fact, a sum of two peaks from two different origin alpha particles, (1) and (4). Peak C represents protons from reaction (3). At this stage of research we could not interpret definitely peak A. Any further analysis requires a construction of a new dedicated measuring bed with possibility to change easily observation angles, shielding foils, etc.

Neutron radiation hardness of the ORTEC preamplifier type 142A was checked in experiment at the MARIA nuclear reactor in the Institute of Atomic Energy POLATOM, Otwock-Świerk. The preamplifier was placed inside channel H8 of the reactor. A pulse generator was connected to the preamplifier. Its output pulse, after amplification by a spectrometry amplifier, was observed. The signal was registered every day by the digitizer card. The output signal amplitude did not change during whole time of the experiment which means that no elements of the preamplifier were damaged. Neutron flux in the experiment was $2.28 \cdot 10^8$ n/cm^2/s. The experiment lasted 5.7 days which gave the dose of $1.13 \cdot 10^{14}$ n/cm^2 neutrons.

Track detectors to detect escaping fast alpha particles

Corresponding author **Adam Szydłowski**
szydlowski@ipj.gov.pl

In order to perform the calibration measurements of the purchased detectors, samples (cut from detector sheets delivered in the three batches) were irradiated with mono-energetic ions of different energies provided by a particle accelerator. During these irradiations the H^+- and D^+- ion energy values were changed in steps of 200 keV in the range from 200 keV to 2 MeV, and for ^{4}He-ions from 300 keV to 5 MeV, and different samples were irradiated with ions of various energies. The irradiated samples were etched in steps in a 6.25 N water solution of NaOH, at a temperature of $70^o \pm 1\ ^oC$ for different etching times. The etching procedure was interrupted every 2 h and track parameters were measured under an optical microscope. After such an analysis the etching process was renewed for a further period of 2 h. The track diameters were measured with an accuracy of ± 0.5 µm.

In Figs 1 there is presented the determined diagrams which show track diameters as a function of ion energy and etching time. The diagrams demonstrate specific maxima, which are shifted to higher ion energies for longer etching times. It was found earlier (A.Szydlowski et al., Nucl. Instr. and Meth. B 171 (2000) 379) that the location of the maximum is defined by the thickness of the external detector layer removed during the bulk etching process, and the range of the projectile in the detector material. It means that tracks are etched out to the largest diameters only when the etching solution has unconstrained access to the end part of the particle trajectory where the concentration of detector material defects is the highest. It takes place after removing (by the etching) of the detector external layer. One can see that the calibration characteristics as determined for each individual detector batch differ significantly one from another (Fig. 1). It means that samples taken from different delivery present craters of different size even when they are irradiated with the same ions and are etched for the same time. It confirms that that various manufacturing procedures were used to produce the detectors. It validates the suggestion that to use the detector in an optimal way a precise calibration of the detectors from each delivery should be performed independently using SSNTDs in tokamak experiments one should take into account that the detectors could operate under harsh conditions of high temperatures and heat impacts. In order to evaluate this effect some alpha-, and proton-irradiated samples were heated in an oven under a controlled temperature for different time periods. The aim of this study was to find possible crater deformations caused by the heating as a function of the temperature and the heating time. After that all the samples were etched under the same standard etching conditions. In Fig. 2 there are shown the diagrams presenting track diameters as a function of the temperature and heating time as measured for the detectors irradiated with α-particles. The diagrams presenting the evolution of proton tracks are very similar to those from Fig. 2. One can conclude that the detectors can be located in a high-temperature environment (e.g. inside a tokamak vacuum vessel) under the condition that the temperature do not exceed 120^o C. Otherwise, a special detector cooling system is needed.

The results of the described studies can be summarized as follows:

1. To make these detectors more useful and better suitable for plasma experiments, and also to find their spectroscopic properties detailed calibration studies are needed for each batch of the PM-355.
2. It was found that the detectors from different bathes can differ significantly and they should be calibrated independently, especially when they are intended to use in spectroscopic measurements.
3. Also the resistance of the detectors irradiated with α-particles and protons to high-temperatures and heat impacts was studied. This experiment has shown that tracks remain unchanged up to temperature of 120 ^{o}C. In the temperature range of 120 ^{o}C – 180 ^{o}C the craters were deformed but they still could be counted. Above 180 ^{o}C the craters disappeared totally. It was also found that the detector in which craters disappeared did not lost its detection properties and it is still sensitive to the ions.

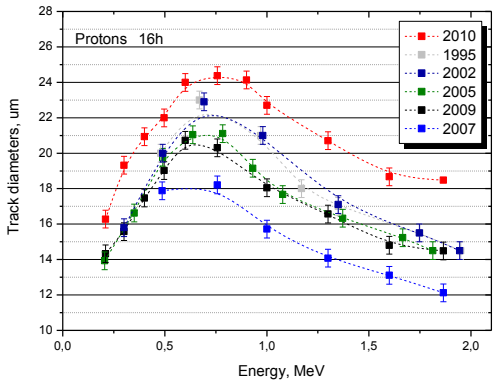

Fig. 1 Evolution of track diameters as a function of incident proton energy and etching time as measured for a few batches of the PM-355 track detector.

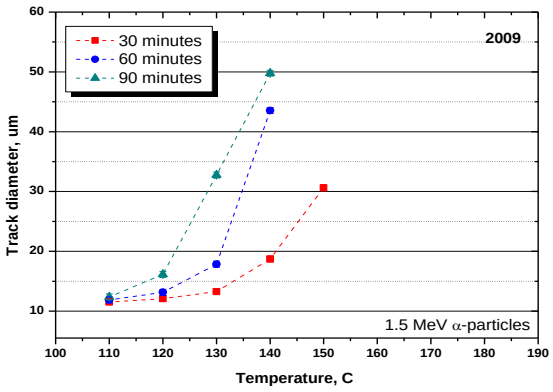

Fig. 2 Evolution of track diameters as a function of temperature for 1.5 MeV α–particles. Etching time – 6h.

Cherenkov detectors for fast electron measurements: new diagnostics for Tore-Supra

Corresponding author **Lech Jakubowski**
lech.jakubowski@ipj.gov.pl

The most important results of the reported studies can be summarized as follows:

For TORE SUPRA: In 2010 the described studies concerned mainly measurements within TORE-SUPRA during the two experimental sessions (in March and October) performed by means of a new Cherenkov-type measuring head of the modified construction. The main idea of that 2010 modification was to change the positions of radiators from the side surface to the front surface of the measuring head. Four diamond radiators enabled to record the fast electron beams of the minimum energies equal to 72 keV, 111 keV, 151 keV and 191 keV, respectively.

The Cherenkov probe enabled the measuring head to be moved into the SOL region along the tokamak small radius, always outside the Last Close Flux Surface (LCFS). During two different experimental campaigns in March and October 2010, the electron-induced signals were much longer than during the first 2009 campaign. The recorded signals were on the level of a few volts. The measurements were performed for different plasma scenarios and discharge regimes, which were especially chosen for ripple-born electrons measurements by means of the Cherenkov type detector. Analysis of experimental results obtained within TORE-SUPRA for the 2008 session were finally presented in paper published in the first quarter of 2010. The most important differences of the new results were changes in the shapes of signals and a considerable increase in intensities of the signals obtained from the Cherenkov radiators in 2010. Intensities of signals were high enough to use an acquisition system installed at the TORE-SUPRA.

During the experimental campaigns, especially in March 2010, the recorded signals made it possible to perform a rough energy analysis of the observed fast electrons stream. Two exemplary sets of signals, which were collected for the single TS plasma discharge during the both experimental sessions in 2010, are presented in Fig. 1. The obtained data enabled us to state that the electron energy E_e in the observed stream was substantially lower than 150 keV, and the electrons of energy ranging from 110 keV to 140 keV gave a big contribution to energetic spectra of the investigated electron stream. An exemplary set of signals from the Cherenkov measuring head, which were obtained during a single TORE-SUPRA discharge in October 2010 and showed the saturation effect, is presented in Fig. 1(B).

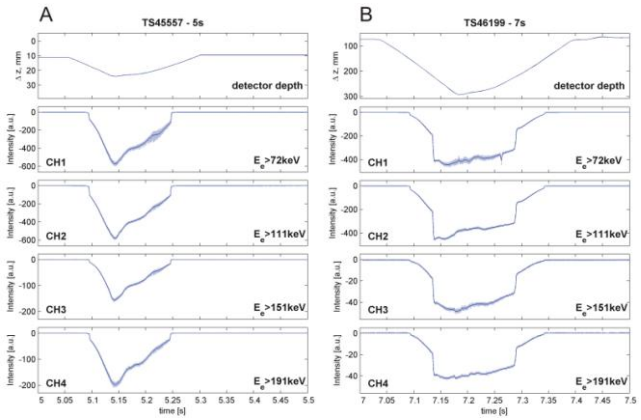

Fig. 1 Set of signals from different channels of the new version of TORE-SUPRA Cherenkov detector, which were recorded for: (A) TS45557 shot - during the action of the reciprocating shaft when the Cherenkov radiators tops reached a distance *d* = 12 cm from the LCFS and (B) TS46199 shot - during the action of the reciprocating shaft when the Cherenkov radiator tops reached a distance of 3.9 cm from the LCFS.

For ISTTOK: As regards the ISTTOK experiment in Lisbon in 2010, the new Cherenkov measuring head equipped with four separate radiators made of AlN crystals, which were thicker than those applied in the 2009 version and which made possible to get stronger electron signals. In 2010 the analysis of experimental results obtained earlier within ISTTOK by means single-channel measuring head and by means prototype multi-channel measuring head were finally published. In the new measuring head the use was made of four AlN crystals of 10 mm in diameter and 2.5 mm in thickness. During the experimental 2010-session the active measuring channels could record electrons of energies higher than about 80 keV (CH1), 120 keV (CH2) and 160 keV (CH3). It was observed that the largest number of fast electrons was recorded in the CH1, while the CH2 and CH3 recorded considerably lower electron numbers. It means that in the run-away emission from the ISTTOK device was dominated by electrons of energy below 120 keV.

Simultaneously, there was investigated the emission of hard X-rays (HXR) outside the ISTTOK chamber in two measuring channels which enabled X-ray energy to be estimated. For this purpose the use was made of two measuring heads equipped with NE102A plastic scintillators of 2.0 cm in diameter and 1.5 cm in length. One measuring head was additionally shielded by a copper plate of 10 mm in thickness. Since the signals were recorded behind different Cu-layers (20 mm and 30 mm, respectively) it was possible to compute the absorption coefficient, which corresponded to X-rays of energy equal to about 400 keV. It could be observed that HXR was probably generated by interactions of the fast electron beams with the limiter, chamber walls and Cherenkov-probe shielding.

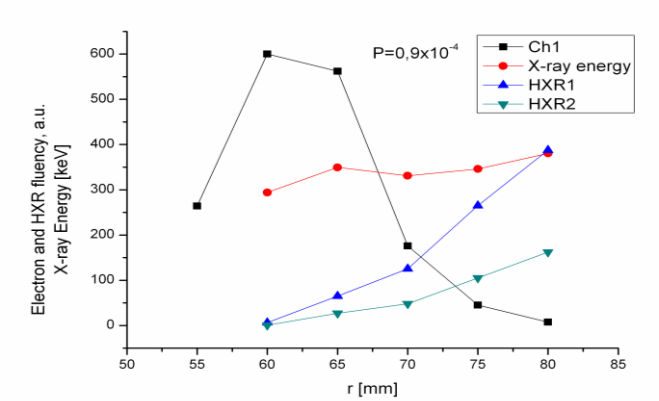

Fig. 2 Fluency of fast electrons (CH1) and X-rays measured behind 20 and 30 mm-thick layer of Cu (HXR1 and HXR2 respectively), determined as a function of the Cherenkov probe position recorded for p_0 = 0.9 x 10^{-4} mbar within ISTTOK. For a comparison there are shown changes in X-ray energies (keV).

Investigation of the run-away electrons within the ISTTOK machine was performed by means of the new Cherenkov measuring head at different positions on the minor radius of the experimental chamber. Those measurements were carried out under different experimental conditions, e.g. at various initial pressures. The example of such a measurements, recorded for $p_0 = 0.9 \times 10^{-4}$ mbar, are shown in Fig. 2.

The obtained diagram showed the maximum electron fluency at r = 60–65 mm, but one should note that the deeper insertion of the probe disturbed the plasma column. The HXR1 and HXR2 signals became stronger when the probe was shifted out the plasma region. In contrary, changes in the HXR energy value showed a weak dependence on the Cherenkov probe position. In the described case the computed HXR energy changed from about 300 keV to about 400 keV.

Preparation of High-Temperature Hall sensor for future applications in measurements of magnetic field in fusion reactors

Corresponding author **Maciej Oszwałdowski**
maciej.oszwaldowski@put.poznan.pl

In our studies in 2010 we were concentrated on three different subjects that are important for the Hall sensors (HS) applicability to the magnetic diagnostics of ITER. They are following.

Hall Sensors radiation resistance

The samples investigated in the present investigations were previously neutron irradiated during Irradiation Nr 3, to the neutron fluence of $1.1*10^{17}$n/cm^2. In the present second irradiation, the fluence was $1.6*10^{18}$ n/cm^2.

Two kinds of samples were investigated: the “worms” and high temperature HSs based on InSb thin films. The worms are InSb films properly shaped to precisely determine the changes in the electrical parameters of InSb films on neutron irradiation. Particularly interesting was the change in the electron concentration of the samples. In view of that purpose the worm-shaped samples had relatively low electron concentration, from $3*10^{16}$cm^{-3} to $8*10^{16}$cm^{-3}. A half of samples of each sort was shielded against the neutron irradiation by InSb-CdTe shields. Unfortunately, for unknown reasons, no shielding effect was observed in the electrical parameters of the samples investigated.

Investigation of the worms revealed that the first irradiation resulted in an increase in the electron concentration by about $2*10^{17}$cm^{-3} and the second irradiation resulted in an increase in the electron concentration by about $2*10^{18}$cm^{-3}. Thus, the increase was proportional to the fluence. The concentration increase has to be attributed to the generation of donor-type defects in the irradiation process. The generated defects effectively decrease the electron mobility. After both irradiations the electron concentration increased from $6.49*10^{16}$cm^{-3} to $2.53*10^{18}$cm^{-3} and the mobility fell down from 22100 cm^2/V*s to 1300 cm^2/V*s. The changes in the electrical parameters are due to the structural defects generated in the InSb during the irradiation.

Sample annealing effectively decreases the number of structural defects, even at as low temperature as 250°C. Therefore, relatively low temperature annealing can be used for the stabilization of the Hall sensors parameters after or during the irradiation process.

The first observation on the HSs is that in the present design they strongly absorb neutrons and their cooling time is long, longer than year. Responsible for that is the silver in the electrical connections. In order to shorten the cooling time to, say, several months, silver must be eliminated from the sensor preparation technology. It can be replaced by gold.

local temperature within HS during the irradiation may be unexpectedly high. Thus, the harsh conditions for the sensors during neutron irradiation may be created both by direct interaction of neutrons with atoms resulting in their transmutation and dislodging and by indirect action through increase in temperature. The matter of the possible strong increase in local temperature should be explained in further investigation.

It was found that in the heavily donor-doped InSb layers, which are the basis of the HSs, the electron concentration is not drastically changed on the second irradiation. It was also found that the sensor package is sufficiently mechanically strong to survive very strong neutron irradiation. Important is also the information that the structural defects introduced to the InSb layer were pretty effectively annealed at relatively low temperatures of 200°C - 300°C. This suggests that low temperature annealing could be used for the recovery of HSs from the defects introduced during the irradiation.

Effect of thermal cycling on Hall sensors parameters

Electric and mechanical properties of HSs can be modified by annealing. In our studies, the annealing procedure was divided into two parts, as shown in the figure below.

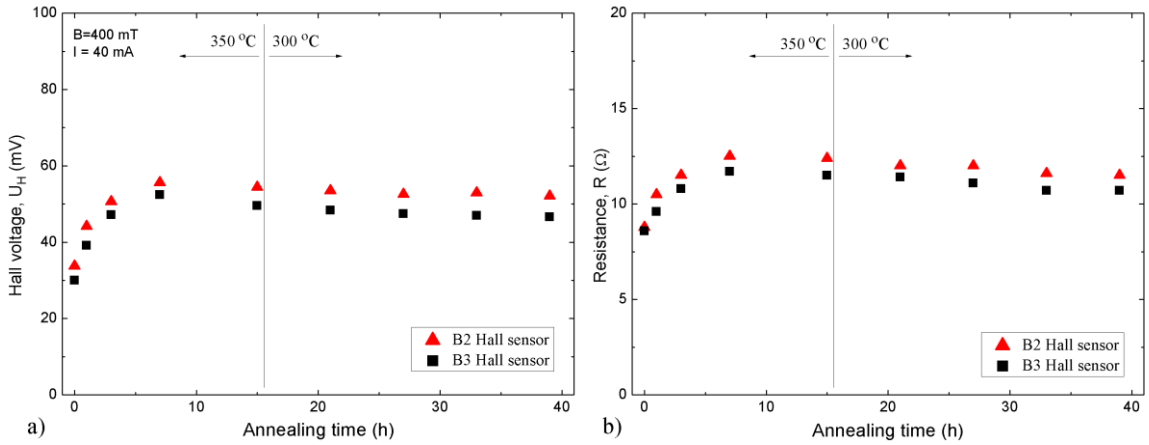

Fig.1 Effect of annealing on two Hall sensors performed at temperatures 350 °C and 300 °C; a) change of Hall voltage U_H, b) change of input resistance R

In the first part, the annealing was performed at 350 °C in air. This annealing lasted 15 h with breaks for performing measurements. This period appeared to be sufficient to roughly stabilize the sensor Hall voltage, U_H, and the resistance, R, as may be concluded from figure above. The temperature of 350 °C, which is above the allowed 300 °C, was applied to accelerate sample stabilization. In the second part, further annealing in air at 350 °C was performed. That annealing lasted up to 39 h. As may be seen in the figure, in this second part changes in the parameters are small, and after 30 h they are practically negligible. The most important conclusion of these investigations is that prolonged annealing at 300°C effectively stabilizes the HS electrical parameters and mechanical strength.

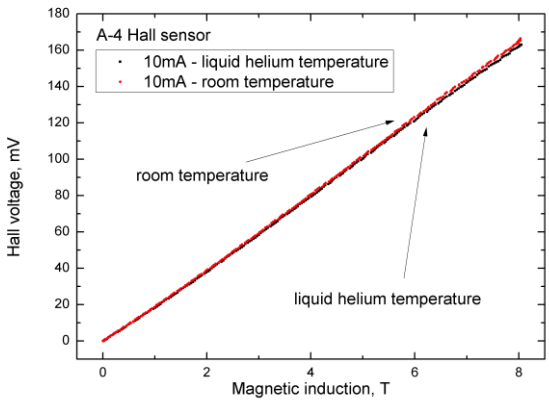

Fig.1 Magnetic field dependence of Hall voltage at room and LH temperatures and driving current I = 10 mA for a typical HS designed for ITER magnetic diagnostics

Studies of HS characteristics in high magnetic fields

These studies are to show that the HSs can effectively be used in the magnetic field range between zero and 10 Tesla, therefore for the magnetic diagnostic of ITER. The magnetic field dependences of Hall voltage of a typical HS is shown in the figure.

Due to the very low temperature coefficient of U_H the dependences for room and LH temperatures are very close. The same dependences are obtained for I = 1 mA and I = 0,1 mA. Below I = 40 mA, $U_H(B)$ does not depend on the driving current.

The HS magnetoresistance also depends on temperature very weakly and does not depend on the driving current. The sensors magnetoresistance is relatively large, and above 2 T, it is roughly linear in *B*. This means that at the high magnetic fields, the HS could be used as a magnetoresistor, which is a two-terminal device (HS is a four-terminal device).

Localized plasma polarimetry based on the phenomenon of normal modes conversion

Corresponding author **Yuri Kravtsov**
y.kravtsov@am.szczecin.pl

Traditional plasma polarimetry, based on the Faraday and Cotton-Mouton effects, provides an information on the line averaged values of plasma density and magnetic field. In contrast to this well known approach an alternative scheme of polarimetric measurement is also available, that makes possible the extraction of local plasma parameters from polarimetric data. The method is based on the phenomenon of normal wave conversion in the vicinity of an orthogonality point, which is the point, where the probing beam is perpendicular to the static magnetic field and mutual transformations of ordinary and extraordinary waves take place. The phenomenon of modes conversion has been extensively investigated since the 1960s, and effectively applied firstly in respect to solar radio emission and then to polarization conversion in the Earth ionosphere plasma.

The evolution of right and left components of the polarization vector $\mathbf{\Gamma} = \Gamma_r \mathbf{e}_r + \Gamma_l \mathbf{e}_l$ in a weakly anisotropic magnetized plasma is described by the coupled equations

$$\frac{\mathrm{d}\Gamma_r}{\mathrm{d}\sigma} = (iG\cos\alpha_\parallel)\Gamma_r + (\tfrac{i}{2}G\sqrt{u}\sin^2\alpha_\parallel)\Gamma_l, \quad \frac{\mathrm{d}\Gamma_r}{\mathrm{d}\sigma} = (\tfrac{i}{2}G\sqrt{u}\sin^2\alpha_\parallel)\Gamma_r + (iG\cos\alpha_\parallel)\Gamma_l, \qquad (1)$$

where $G = k_0 v\sqrt{u}/2$ is a combination of a wave number $k_0 = \omega/c$ and standard plasma parameters $v = 4\pi e^2 N_e / m\omega^2$ and $u = \left(eB_0/mc\omega\right)^2$. Accepting linearized model for $\cos\alpha_\parallel$, presented in [2] one can express solution of the QIA equations (9) in terms of parabolic cylinder functions and then to find the coefficient of conversion of the right hand polarized wave into the left hand wave:

$$\eta(\text{right hand} \to \text{left hand}) = 1 - \exp(-\pi p/4), \qquad (2)$$

where

$$p = Gu|\rho_B| = \tfrac{1}{2}k_0 v u^{3/2}|\rho_B| = \frac{2\pi e^5}{m^2c^4}\frac{qR^2}{2h}\frac{N_e B_0^3}{\omega^4}. \qquad (3)$$

Having measured the transformation coefficient η experimentally, one can find the plasma parameter p from the formula

$$p = -(4/\pi)\ln(1-\eta). \qquad (4)$$

Thus, in case of spatial localization the coefficient of modes conversion η provides information on combination of plasma parameters $N_e B_0^3$ at the point of orthogonality.

Considering limitations inherent to localized polarimetric measurements, we restrict ourselves by the following four points.

First off all, conversion coefficient η should be "measurable", that is not very small and sufficiently different from a unit. Specifically we have taken $0.05 < \eta < 0.95$. Secondly, the normal modes have to be independent outside the area of interaction. Independence of normal Iodes implies that beating interval between normal modes is small as compared with characteristic length of plasma inhomogeneity. Thirdly, for applicability of Quasi-isotropic Approximation plasma should manifest the properties of weakly anisotropic medium. Fourthly, the localization lint of normal modes conversion area should satisfy inequality $l_{\text{int}} << a$. Specifically we have chosen $l_{\text{int}} = 30\,\text{cm}$ and $a = 3\,\text{m}$.

All these four limitations leads to restrictions of the beam frequency range and measurable plasma density values, admissible for localized polarimetric measurement. Detailed estimates, based on the plasma parameters typical for ITER, could be expressed by a set of equations:

$$\begin{cases} N_{1\min}(\omega) \equiv 4.17 \cdot 10^{-38} \omega^4 < N_e < 2.44 \cdot 10^{-36} \omega^4 \equiv N_{1\max}(\omega) \\ N_{2\min}(\omega) \equiv 1.1 \cdot 10^{-12} \omega^2 < N_e < 1.8 \cdot 10^{-21} \omega^3 \equiv N_{3\max}(\omega) \\ \omega > \omega_{\min} = 3.17 \cdot 10^{13}\ \text{rad} \cdot \text{s}^{-1} \end{cases} \quad (5)$$

and are presented at Fig.1. The range, satisfying all limitations (5), is marked by the green area.

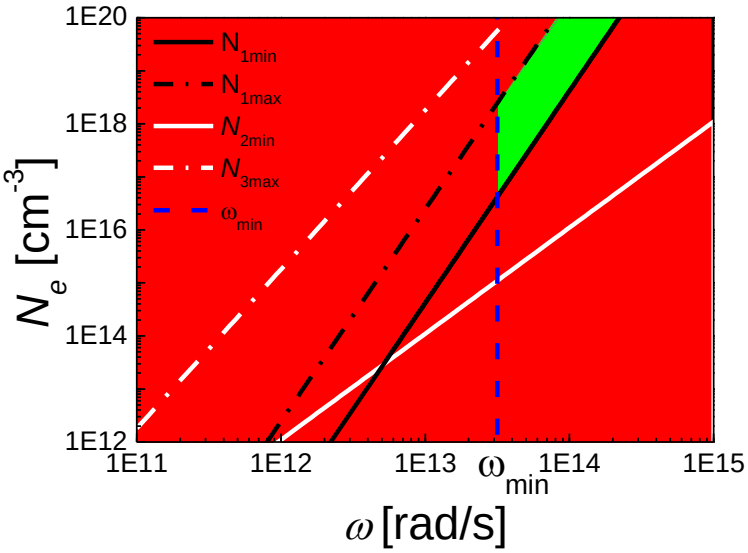

Fig. 1 The plasma densities, admissible for localized measurements

The minimum measurable value of electron density $N_{e\,\min}$ happens to be as high, as $10^{17}\ \text{cm}^{-3}$. This density is thousand times higher than maximum densities, planned by ITER project. Thus, the method of localized microwave polarimetry, which have proved its efficiency in the ionospheric studies, happens to be inapplicable to the toroidal plasma in the ITER project. This analysis also limits the applicability of localized polarimetry in the other thermonuclear devices like JET or W-7X.

Development of gas detectors for 2.5 and 14 MeV neutron measurements utilizing activation method

Corresponding author **Marek Scholz**
marek.scholz@ipplm.pl

The idea of the counter based on detection the charged particles produced in the following reaction $^{9}Be + n \rightarrow \alpha$ (1.0 MeV) + $^{6}He(T_{1/2}=0.8\ s) \rightarrow {}^{6}Li + \beta^{-}$ (1.5 MeV).
The prompt alpha particles or delayed beta particles can be recorded. Because the prototype of the counter has been tested on the PF-1000 device with neutron pulse taking a few ns, we decided to record the beta particles. The proportional detector (Canberra SP-126C filled with P-10, i.e. Ar-90%+CH_4-10%) equipped with beryllium plate (2 x 100 x 100 mm, 1.8 g/cm^{-3}) has been chosen.

In order to prepare the counter calibration, the MCNP calculations have been performed. The MCNP input needed to calibration of the detector is presented in Fig. 1.

The following steps of the proportional counter calibration procedure have been done:

- Simulation the ^{6}He beta spectrum inside the counter (MCNP);
- Shaping the ^{90}Sr/^{90}Y beta calibration source spectrum (MCNP);
- Calculation the counter response to ^{90}Sr/^{90}Y calibration source;
- Measurements of the counter response to ^{90}Sr/^{90}Y calibration source (10x10cm);
- Obtaining of „calculation to experiment" (C/E) ratio for ^{90}Sr/^{90}Y source;
- Simulation of the counter response to ^{6}He source in beryllium;
- Application of C/E ratio for ^{90}Sr/^{90}Y source to the beta ^{6}He source simulations;
- Simulation of beryllium plate response to neutron source (MCNP);
- Obtaining efficiency of the Beryllium Activation Counter;
- Testing measurements on PF-1000.

The simulation of energy spectrum the beta particles coming from beryllium activation as it occurs inside the counter is presented on the Fig. 1 (dark blue line).

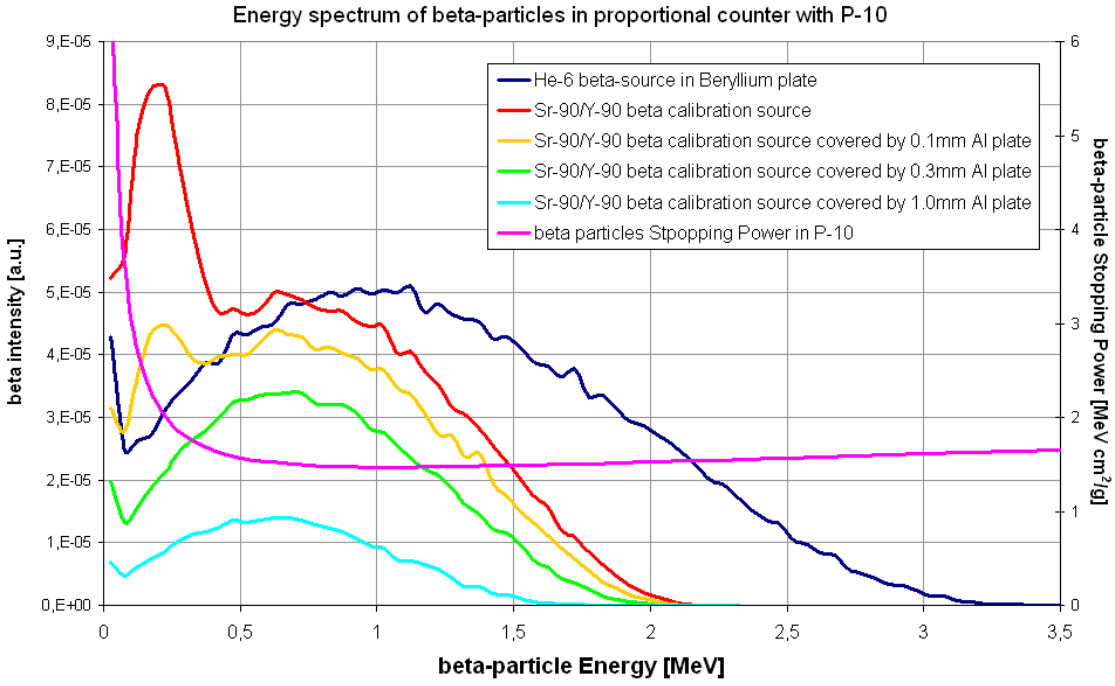

Fig. 1

The calibration of the counter has been performed by means of the $^{90}Sr/^{90}Y$ source with energy spectrum shown as red line on the Fig. 1. In order to make it similar to the ^{6}He source, the spectrum has been shaped using aluminium plate with different thickness. The 0.3 mm thick aluminium plate has been selected (green line on Fig. 1).

The electronic components essential to the proportional counter containing beryllium target and data acquisition system have been prepared (see Fig. 2).

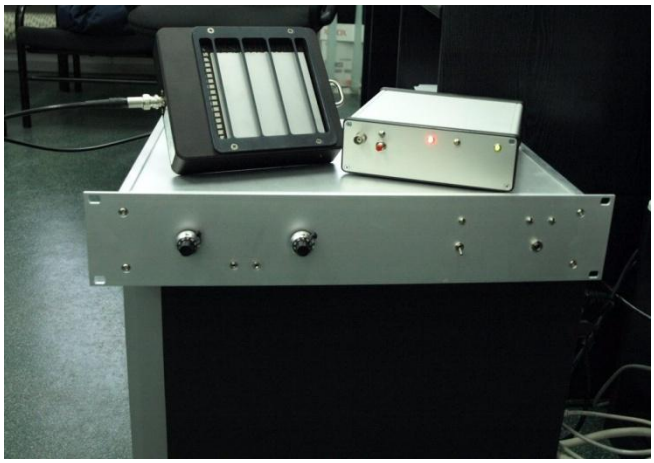

Fig. 2

The system includes:

- Two separate channels for two proportional counters
- Battery operated preamplifiers with fibre optics links to the computer in order to avoid the electro-magnetic noises and interference problems

Preamplifier – Discriminator settings: sensitivity - 105 electrons, dead time - 0.5 μs, output pulse width - 250 ns. HV power supply with output voltage 1650 V. Two independent gating times for both channelsA series of measurements by means of the Beryllium Activation Counter have been performed during the experimental campaign on PF-1000 device.

3.5 Inertial fusion energy "keep-in-touch" activity

Analysis of emerging options of IFE on the basis of results of experiments and numerical modelling

Corresponding author **Tadeusz Pisarczyk**
tadeusz.pisarczyk@ipplm.pl

The experiment was carried out at the Prague Asterix Laser System. The investigations were aimed at testing the possibility of plasma jet creation by using different constructions of targets with conically shaped thin foils. Fig. 1. The cones were irradiated directly or indirectly by a focused pulsed high-power laser beam. In the investigations the following target irradiation parameters were used: the first harmonic of laser radiation (λ=1.315 μm), laser energies 120 and 600 J, and pulse duration 250 ps (full width at half maximum).

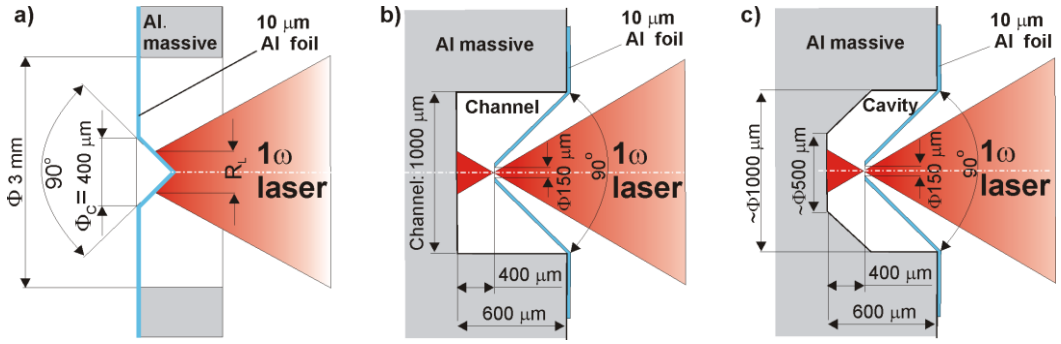

Fig. 1. The target constructions with a conically shaped thin foil: a) – target with direct cone irradiation, b) - double target with free ablative plasma expansion (TF), and c) - double target with pressure cavity (TP)

Our interferometric investigations show that in the case of the direct cone irradiation (Fig. 1a). The initial axial velocity of plasma contour reaches a value lying in the range of (5-8)x10^7 cm/s, however it drops very fast below 2x10^7 cm/s.

To improve the plasma jest parameters we tested the possibility to accelerate the foils by exploiting the ablative plasma pressure: (i) Reverse Acceleration Scheme and (ii) Cavity Pressure Acceleration Scheme method. Two new target constructions were designed: (i) double target with free ablative plasma expansion (TF) and (ii) double target with pressure cavity (TP), as presented in Fig. 1b and Fig. 1c, respectively. The performed experiments with both the targets types show that the plasma jets parameters are considerably better than those obtained with direct cone irradiation at the same laser energy. The average plasma jet velocities in the observation period are higher than 10^7 cm/s, whereas in the direct irradiation case the velocity was decreasing very fast below that value. Moreover, it should be emphasized that the maximum electron density in the jets is twice higher than in the case of the direct cone irradiation. However, the plasma jet propagation starts with a longer delay (several ns), which is characteristic for both TP and TF targets.

The investigations of plasma stream parameters for the three target constructions used allowed us to come to the conclusion that a proper ratio of the laser energy part used for heating to that exploited for acceleration of the cone wall is very important for launching a good-quality jet. If a majority of laser energy is used for the cone wall heating, the collapse of the cone is not effective, whereas in the opposite case the too fast acceleration of the cone wall results in conservation of its steady state and in subsequent cone reversal and destruction. However, in the case of TP target there is a certain possibility to control the above energy ratio by means of fitting the cavity volume to target irradiation parameters.

For that reason some additional numerical modeling will be very useful. In the case of indirect methods of plasma jet generation a certain disadvantage may consist in some delay of the plasma jet creation.